SUPPORTING INFORMATION

DNA-Scaffolded Synergistic Catalysis

Edward B. Pimentel,[1] Trenton M. Peters-Clarke,[1] Joshua J. Coon,[1,2,3,4] and Jeffrey D. Martell[1,5]*

[1] Department of Chemistry, University of Wisconsin-Madison, Madison, WI, 53706, USA
[2] Department of Biomolecular Chemistry, University of Wisconsin-Madison, Madison, WI, 53706, USA
[3] National Center for Quantitative Biology of Complex Systems, Madison, WI, 53706, USA
[4] Morgridge Institute for Research, Madison, WI, 53515, USA
[5] Carbone Cancer Center, University of Wisconsin School of Medicine and Public Health, Madison, WI, 53705, USA
* jdmartell@wisc.edu

General Information S2
DNA Sequences S4
Synthesis and Characterization S6
General Procedure for Bioconjugation of a Bipyridine Ligand to DNA S6
Characterization of Bipyridine-DNA Conjugates (Figures S1-S9) S7
General Procedure for Bioconjugation of a Nitroxyl Radical to DNA S12
Characterization of TEMPO-DNA Conjugates (Figures S10-S12) S13
Synthesis of 6-methoxy-2-naphthalenemethanol (Figures S13-S14) S15
Supplemental Experiments (Figures S15-S30) S17
Estimating Effective Concentration (Figure S31) S33
Supplemental Note: Mechanism of Cu/TEMPO Oxidation S36
References S37

General Information

Materials

All solvents used in this study were purchased from Sigma Aldrich in HPLC Grade and used without further purification. All reagents were purchased from TCI, Fisher, Sigma Aldrich, Santa Cruz Biotechnology, Alfa Aesar, or Ambeed and used without further purification. Unmodified and amine-modified DNA oligonucleotides were purchased from Integrated DNA Technologies with standard desalting.

HPLC Analysis and Purification

Reverse-phase HPLC analysis and purification of DNA conjugates and reverse-phase HPLC reaction tracking were performed on a Shimadzu Prominence HPLC system with quantification at 254 nm. HPLC analysis and purification of DNA oligonucleotides was performed using a 4.0 × 300 mm Kromasil 100-5-C18 column with 1.0 mL/min flow under ion-pairing conditions using aqueous 100 mM triethylammonium acetate pH 7.0 (TEAA) as mobile phase A and acetonitrile as mobile phase B (using a gradient from 10–30% B over 10 minutes, followed by a 1 minute ramp to 90% and a 1 minute wash at 90% B and then re-equilibration at 10% B), with a column oven temperature of 50 °C. HPLC reaction tracking of alcohol oxidation was performed using a 4.6 × 50 mm XBridge C18 (3.5 μm) column with 1.0 mL/min flow using water with 0.1 % trifluoroacetic acid as mobile phase A and acetonitrile as mobile phase B, with a column oven temperature of 30 °C (using a gradient from 10–90% B over 5 minutes, followed by a 1.5 minute wash at 90% B and then re-equilibration at 10% B). The differences in absorbance at 254 nm for each substrate and product were accounted for by construction of calibration curves in triplicate in the linear range of each compound.

NMR Spectroscopy

^{1}H and $^{13}C\{^{1}H\}$ NMR spectra were recorded on a Bruker Avance 500 MHz spectrometer. Chemical shifts (δ) are given in parts per million and referenced to TMS.

UV-Vis Spectroscopy

DNA concentrations were determined by UV-Vis spectroscopy (absorption at 260 nm) using a Nanodrop One Spectrophotometer (ThermoFisher Scientific).

Mass Spectrometry

All MS and MS/MS experiments were performed on a quadrupole-Orbitrap-quadrupole linear ion trap (q-OT-QLT) hybrid mass spectrometer system (Orbitrap Fusion Lumos, Thermo Fisher Scientific, San Jose, CA) that was modified to perform negative electron transfer dissociation (NETD).[1] To boost generation of sequence informative fragment ions during tandem MS, the mass spectrometer was modified to include a Firestar Ti-60 Synrad 60 W CO_2 continuous wave laser to allow for the photoactivation of DNA anions during the ion-ion reaction.[2] Following purification with ion-exchange HPLC, samples were diluted to 5 μM of ssDNA-co-catalyst conjugate in 70% acetonitrile and 30% nuclease-free water with 10 mM ammonium acetate. Solutions were pH-adjusted to pH 9.5 with ammonium hydroxide. The ssDNA-co-catalyst conjugate samples were directly infused at a flow rate of 3 μL/min, and anions were generated via electrospray in the negative ion mode with a heated electrospray voltage of −2.2 kV relative to ground and a transfer tube temperature of 300 °C. The ion funnel RF was held at 60%. All MS survey spectra were collected at a resolving power of 500,000 at 200 *m/z* in the Orbitrap with a scan range of 400–

3,000 *m/z*, an AGC target of 400,000 charges and a maximum injection time of 50 ms. To aid in desolvation, nitrogen sheath and auxiliary gas were applied at 15 and 10 arbitrary units, respectively. MS/MS experiments were briefly carried out to confirm the identity of putative adducted species. After a 30 ms NETD reaction with fluoranthene radical cations (reagent AGC target = 100,000), all product ions and unreacted precursor ions were shuttled to the ion routing multipole for beam-type collisional dissociation at 25 normalized collisional energy (NEThcD) and scanned out in the Orbitrap with resolving power of 240,000 at 200 *m/z*. Upon fragmentation, no site-specificity was determined for adducts. All MS and MS/MS data were collected in profile mode. For increased signal-to-noise (S/N), MS spectra are the sum of 50 individual scans, with averaging performed in the vendor's post-acquisition software (XCalibur Qual Browser, version 2.2). No microscans were performed.

Gel Electrophoresis

2% agarose gels (cast with 3 μL of a 10 mg/mL aqueous stock of ethidium bromide for every 50 mL of molten gel solution, for DNA visualization) were prepared in 1x TAE buffer and run for 40 minutes at 120 V. Gel images were recorded on an Azure C400 Gel Imaging System (Azure Biosystems) using 302 nm transillumination.

Fluorescence Reaction Tracking

Fluorescence experiments were recorded on a Tecan Spark fluorescence plate reader with the following conditions: 350 nm excitation wavelength with a 5 nm bandwidth, 450 nm emission wavelength with a 10 nm emission bandwidth, 30 flashes with an integration time of 40 μs, and no delay time.

General Procedure for DNA-Scaffolded Aerobic Oxidation of Benzylic Alcohols

2 nmol (0.5 mol %) of each complementary DNA-co-catalyst conjugate and any unmodified templating strands were diluted to 100 μM in 100 mM borate buffer pH 9.5 with 100 mM NaCl in a 1.5 mL centrifuge tube. The DNA assembly was then thermally annealed by heating for 2 minutes at 92 °C, followed by cooling to room temperature. Acetonitrile was added (sufficient to bring the total reaction volume to 40 μL after addition of CuBr and substrate), followed by 2 nmol of CuBr as a 1 mM CuBr stock in acetonitrile and 400 nmol of alcohol substrate as a 100 mM stock in acetonitrile. The reaction was then vortexed and spun down using a table-top microcentrifuge to ensure thorough mixing, and then incubated at 20 °C with 900 rpm shaking for the duration of the reaction. Reaction tracking was performed by HPLC: at each timepoint, the reaction was vortexed and spun down, and then a 2 μL aliquot was diluted with 40 μL of 1:1 MeOH/100 mM triethylammonium acetate buffer pH 7.0 in an HPLC vial insert. This sample was then analyzed by reverse-phase HPLC as described above. Yields were calculated by integrating chromatogram peaks from the chromatogram generated using UV absorbance at 254 nm and corrected for individual analyte response using calibration curves for each substrate and product.

Unscaffolded reactions and reactions containing exogenous co-catalysts were prepared as above. The 4,4′-dicarboxybipyridine ligand (dissolved in aqueous 100 mM borate buffer pH 9.5) was added to the aqueous sample prior to thermal annealing, and the 4-carboxy-TEMPO co-catalyst was added as a 1 mM stock in acetonitrile along with the CuBr and substrate.

DNA Sequences

All sequences used in this paper are listed below, each named using a unique identifying code of the form *dna##*. Co-catalyst conjugates prepared are referred to by the original sequence and the attached molecule (e.g. *dna##+dcbpy* or *dna##+cTEMPO*). /3AmMO/ and /5AmMC6/ are codes used by the DNA supplier (Integrated DNA Technologies) to refer to amino-modifications positioned at the 3′ and 5′ ends of synthetic oligonucleotides.

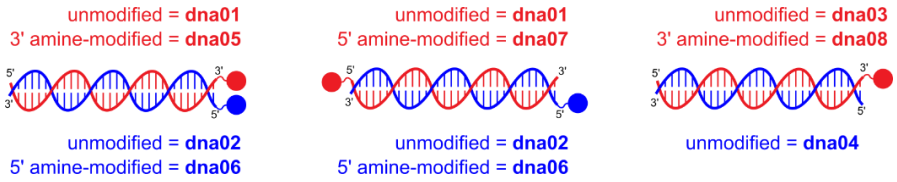

Sequences used in Figures 2 and 3

dna01 = 5′-ACAGGCTAACGAACGATCTCGAGCGC-3′
dna02 = 5′-GCGCTCGAGATCGTTCGTTAGCCTGT-3′
dna03 = 5′-CGTAGTGAGACTTACAGCTTCGTAGG-3′
dna04 = 5′-CCTACGAAGCTGTAAGTCTCACTACG-3′
dna05 = 5′-ACAGGCTAACGAACGATCTCGAGCGC-/3AmMO/-3′
dna06 = 5′-/5AmMC6/-GCGCTCGAGATCGTTCGTTAGCCTGT-3′
dna07 = 5′-/5AmMC6/-ACAGGCTAACGAACGATCTCGAGCGC-3′
dna08 = 5′-CGTAGTGAGACTTACAGCTTCGTAGG-/3AmMO/-3′

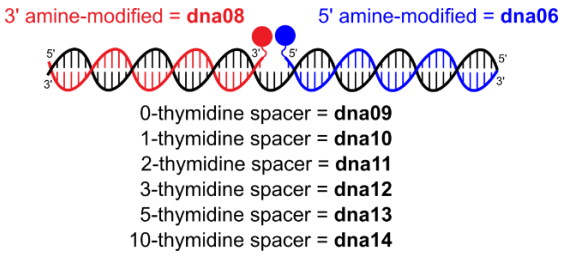

Sequences used in Figure 4

dna06 = 5′-/5AmMC6/-GCGCTCGAGATCGTTCGTTAGCCTGT-3′
dna08 = 5′-CGTAGTGAGACTTACAGCTTCGTAGG-/3AmMO/-3′
dna09 = 5′-
ACAGGCTAACGAACGATCTCGAGCGCCCTACGAAGCTGTAAGTCTCACTACG-3′
dna10 = 5′-
ACAGGCTAACGAACGATCTCGAGCGCTCCTACGAAGCTGTAAGTCTCACTACG-3′
dna11 = 5′-
ACAGGCTAACGAACGATCTCGAGCGCTTCCTACGAAGCTGTAAGTCTCACTACG-3′
dna12 = 5′-
ACAGGCTAACGAACGATCTCGAGCGCTTTCCTACGAAGCTGTAAGTCTCACTACG-3′

dna13 = 5′-
ACAGGCTAACGAACGATCTCGAGCGCTTTTTCCTACGAAGCTGTAAGTCTCACTACG
-3′
dna14 = 5′-
ACAGGCTAACGAACGATCTCGAGCGCTTTTTTTTTTCCTACGAAGCTGTAAGTCTCA
CTACG-3′

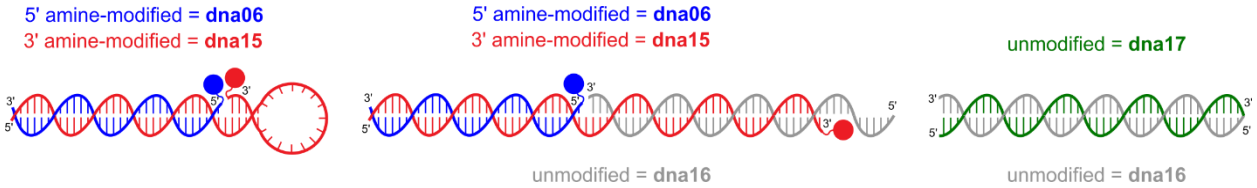

Sequences used in Figure 5
dna06 = 5′-/5AmMC6/-GCGCTCGAGATCGTTCGTTAGCCTGT-3′
dna15 = 5′-
ACAGGCTAACGAACGATCTCGAGCGCGCGAGAAGTTAAGACCTATGCTCGC-
/3AmMO/-3′
dna16 = 5′-CCTGAACCGCGAGCATAGGTCTTAACTTCTCGC-3′
dna17 = 5′-GCGAGAAGTTAAGACCTATGCTCGCGGTTCAGG-3′

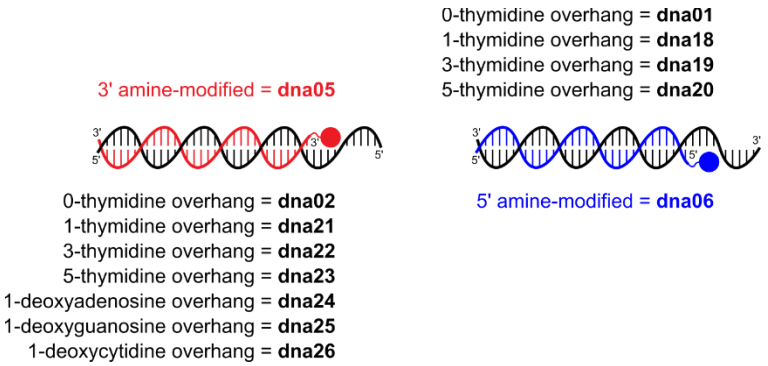

Sequences used in Figures S24-27
dna01 = 5′-ACAGGCTAACGAACGATCTCGAGCGC-3′
dna02 = 5′-GCGCTCGAGATCGTTCGTTAGCCTGT-3′
dna05 = 5′-ACAGGCTAACGAACGATCTCGAGCGC-/3AmMO/-3′
dna06 = 5′-/5AmMC6/-GCGCTCGAGATCGTTCGTTAGCCTGT-3′
dna18 = 5′-ACAGGCTAACGAACGATCTCGAGCGCT-3′
dna19 = 5′-ACAGGCTAACGAACGATCTCGAGCGCTTT-3′
dna20 = 5′-ACAGGCTAACGAACGATCTCGAGCGCTTTTT-3′
dna21 = 5′-TGCGCTCGAGATCGTTCGTTAGCCTGT-3′
dna22 = 5′-TTTGCGCTCGAGATCGTTCGTTAGCCTGT-3′
dna23 = 5′-TTTTTGCGCTCGAGATCGTTCGTTAGCCTGT-3′
dna24 = 5′- AGCGCTCGAGATCGTTCGTTAGCCTGT -3′
dna25 = 5′- GGCGCTCGAGATCGTTCGTTAGCCTGT -3′
dna26 = 5′- CGCGCTCGAGATCGTTCGTTAGCCTGT -3′

Synthesis and Characterization

General Procedure for Bioconjugation of a Bipyridine Ligand to DNA

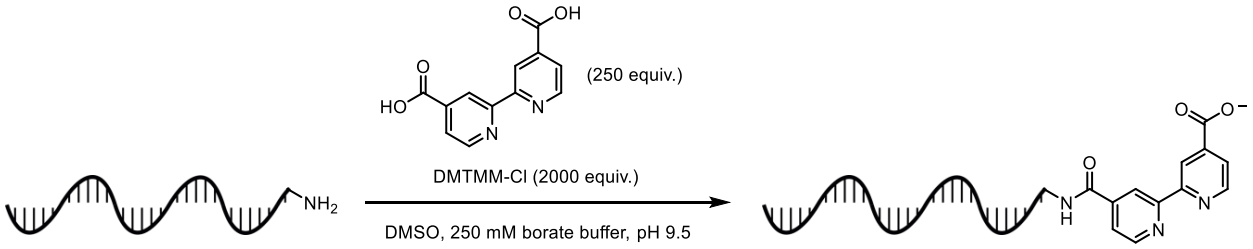

In a 1.5 mL centrifuge tube, 100 nmol of amine-modified DNA oligonucleotide (10 mM stock in nuclease-free water) was diluted with 290 μL of 250 mM sodium borate buffer, pH 9.5 and 100 μL of DMSO. 100 μL of a 0.25 M stock of 4,4′-dicarboxy-bipyridine (dcbpy, in 1:1 250 mM sodium borate buffer, pH 9.5 and DMSO, 250 equivalents), was then added, followed by 400 μL of 0.5 M DMTMM-Cl (in nuclease-free water, 2000 equivalents). The sample was vortexed thoroughly, spun down in a bench-top centrifuge, and then incubated for 16 hours at 17 °C with 500 rpm shaking in an Eppendorf thermomixer. At this point, the sample was spun down to pellet any precipitate and then concentrated by transferring the supernatant to and concentrating in a 3K Amicon Ultra-0.5 mL centrifugal filter device (prerinsed with 500 μL of nuclease-free water and spun down at 14000 rcf for 10 minutes, then loaded with sample and concentrated by spinning as before). The device was then diluted with 400 μL nuclease-free and concentrated by spinning as before, three times to remove residual ligand. The retentate was recovered and the membrane was rinsed with 50 μL nuclease-free water to maximize recovery. The concentration of crude DNA-conjugate was then checked by UV absorption at 260 nm using a NanoDrop spectrometer. The isolated conjugate was then purified by HPLC by iterative injection of 20 nmol aliquots. The product-containing fractions were then pooled, lyophilized, buffer-exchanged with nuclease-free water on a second Amicon Ultra filtration device to remove residual TEAA from the HPLC purification, and then subjected to a final lyophilization before resuspension in nuclease free water to approximately 1 mM concentration. The final concentration of conjugate was determined using a NanoDrop spectrometer. Yields ranged from 35–80 nmol of HPLC-purified DNA conjugate. To assess the integrity of oligonucleotide-co-catalyst conjugates, intact mass analysis via electrospray mass spectrometry (ESI-MS) was performed (see “Mass Spectrometry”).

Characterization of Bipyridine-DNA Conjugates

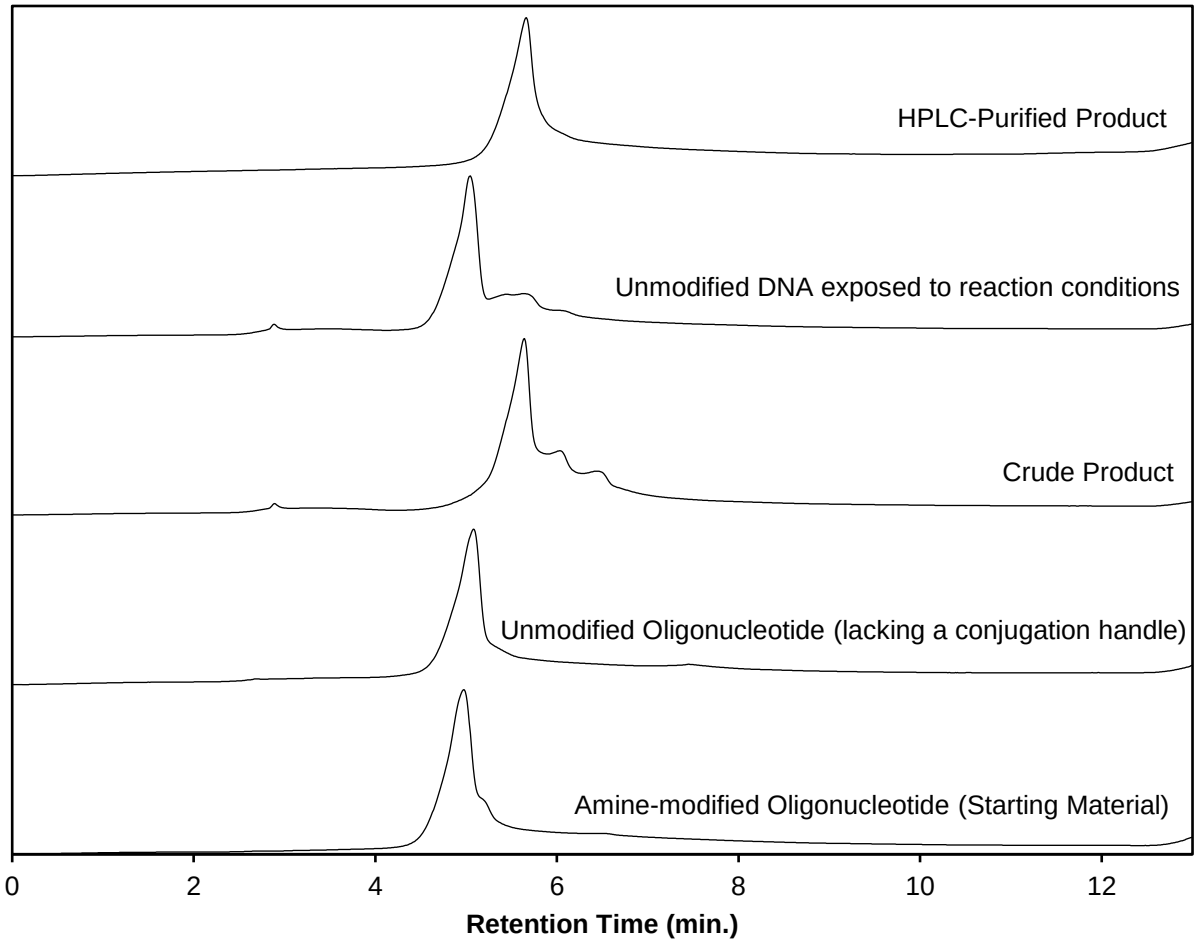

Figure S1. HPLC Analysis of the bioconjugation of 4,4′-dicarboxy-2,2′-bipyridine to DNA. Subjection of an amine-modified DNA oligonucleotide (dna05) to bioconjugation conditions led to near complete consumption of the starting material oligo, and generation of one major product with a few minor impurities. The control reaction using DNA that lacks a conjugation handle (dna01) showed minor product peaks, suggesting that there is non-negligible modification of the native DNA strand, perhaps through covalent modification of nucleobase amine functional groups. Subsequent HPLC purification allowed for the isolation of the major product from these undesired, multiply-modified impurities.

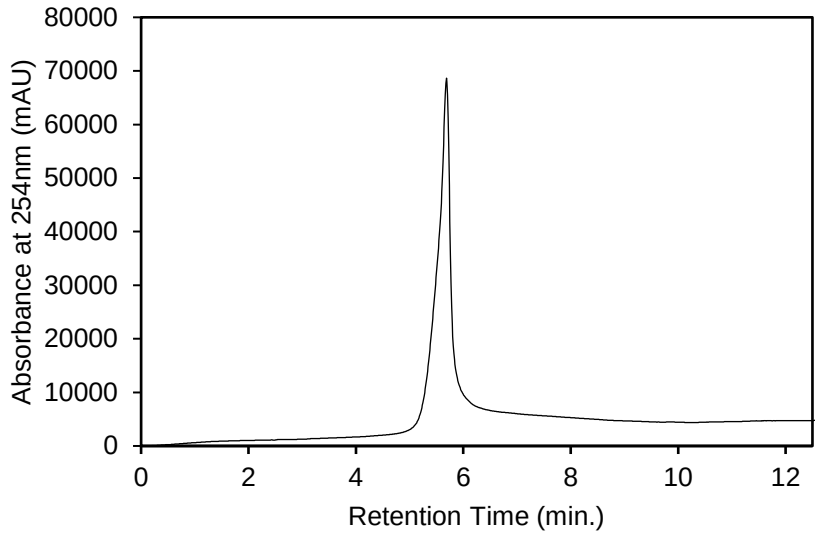

Figure S2. HPLC chromatogram of HPLC-purified dna05+dcbpy using absorbance at 254 nm. 10 μL of 0.2x DNA-conjugate stock were injected for analysis.

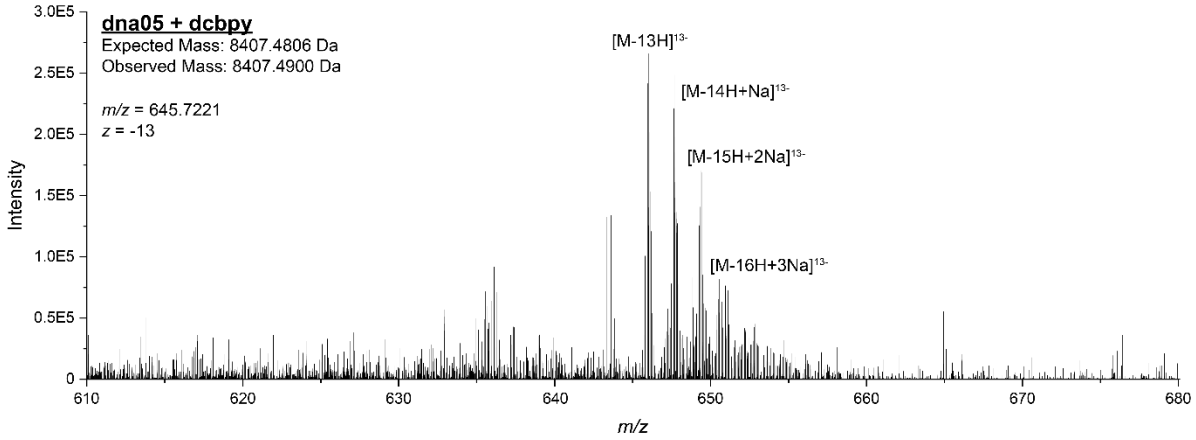

Figure S3. Electrospray mass spectrum for the HPLC-purified dna05+dcbpy conjugate. A negative-mode, high-resolution MS^1 spectrum, representing the average of 50 scans, is shown for the ssDNA-co-catalyst analyte. The expected monoisotopic mass for the conjugate, including the 26-nucleotide single-stranded DNA sequence dna05 and a single 4,4′-dicarboxybipyridine (dcbpy) co-catalyst bound at the 3′-terminus, is shown. The observed monoisotopic mass, calculated by deconvolution of the observed $z = -13$ precursor (m/z = 645.7221), is also shown. Moderately abundant adducted species, including the expected conjugate with sodium and ammonium adducts, are additionally labeled.

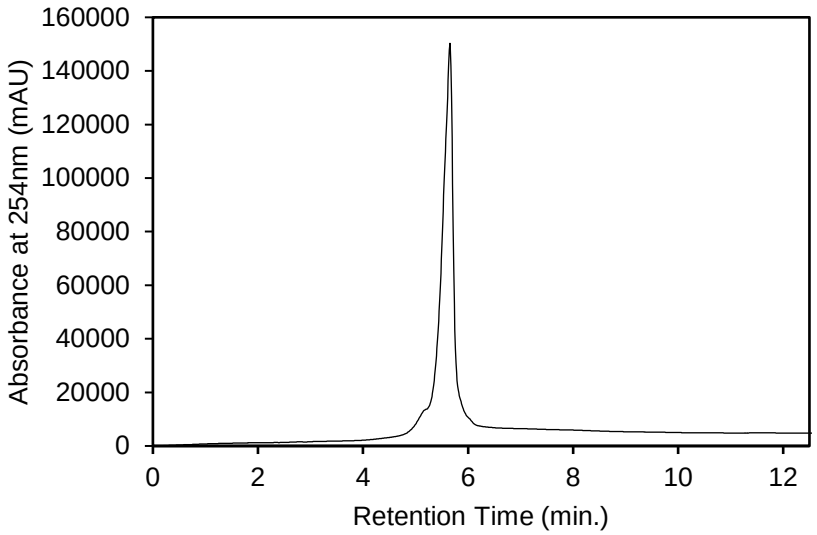

Figure S4. HPLC chromatogram of HPLC-purified dna08+dcbpy using absorbance at 254 nm. 10 μL of 0.2x DNA-conjugate stock were injected for analysis.

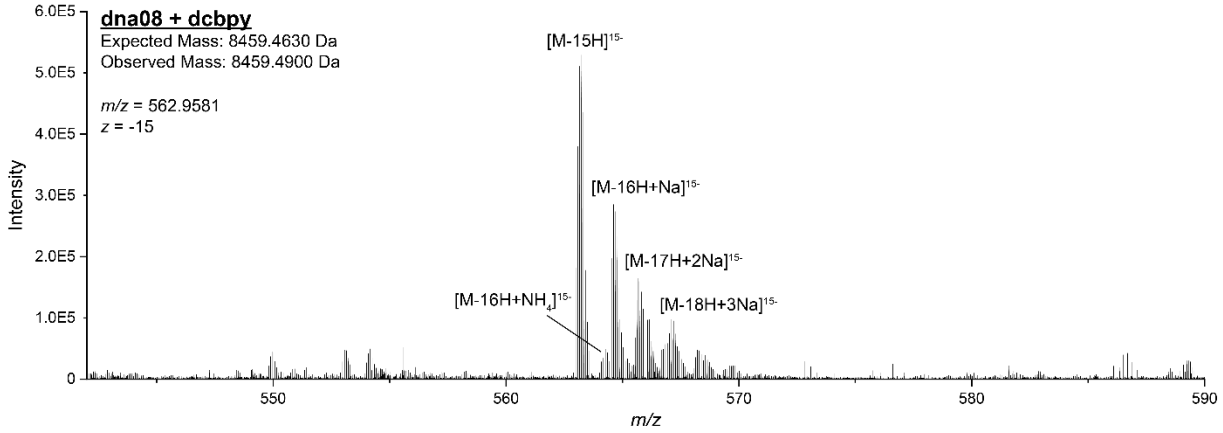

Figure S5. Electrospray mass spectrum for the HPLC-purified dna08+dcbpy conjugate. A negative-mode, high-resolution MS^1 spectrum, representing the average of 50 scans, is shown for the ssDNA-co-catalyst analyte. The expected monoisotopic mass for the conjugate, including the 26-nucleotide single-stranded DNA sequence dna08 and a single 4,4′-dicarboxybipyridine (dcbpy) co-catalyst bound at the 3′-terminus, is shown. The observed monoisotopic mass, calculated by deconvolution of the observed $z = -15$ precursor (m/z = 562.9581), is also shown. Moderately abundant adducted species, including the expected conjugate with sodium and ammonium adducts, are additionally labeled.

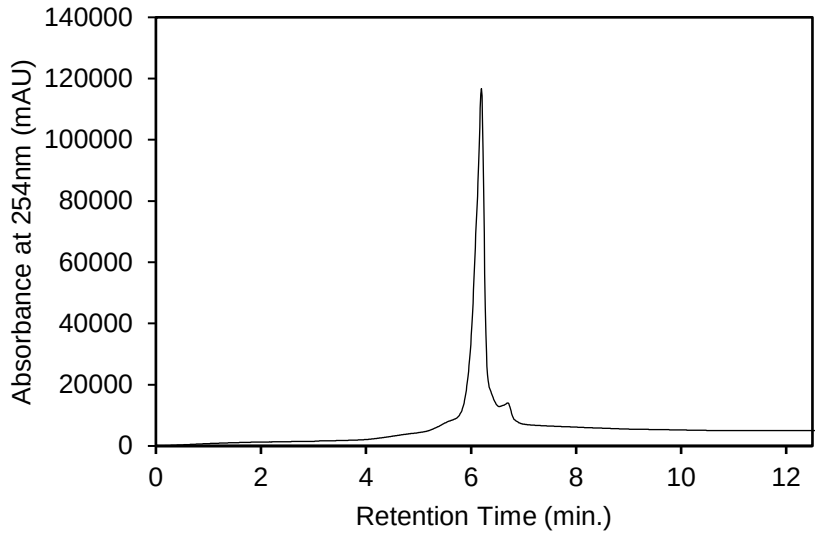

Figure S6. HPLC chromatogram of HPLC-purified dna07+dcbpy using absorbance at 254 nm. 10 μL of 0.2x DNA-conjugate stock were injected for analysis.

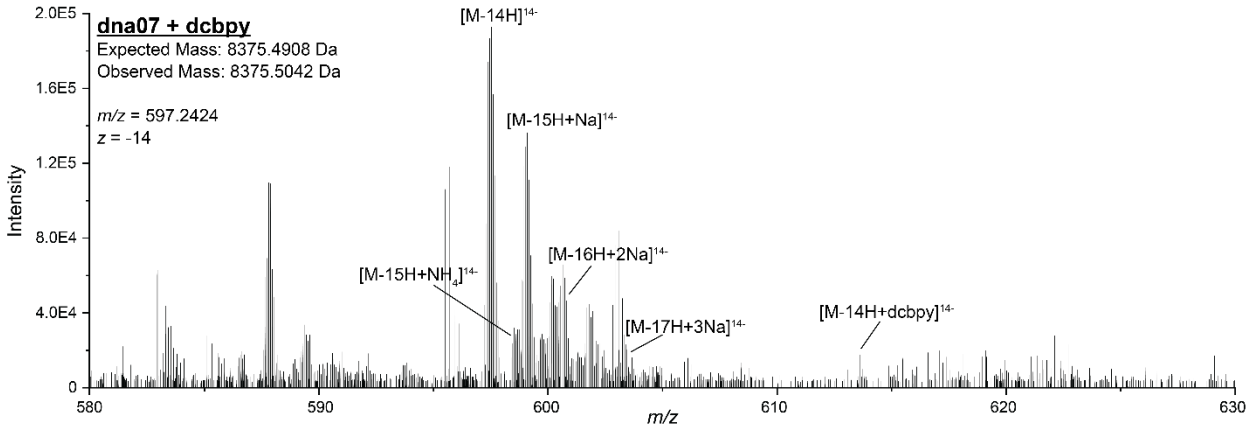

Figure S7. Electrospray mass spectrum for the HPLC-purified dna07+dcbpy conjugate. A negative-mode, high-resolution MS^1 spectrum, representing the average of 50 scans, is shown for the ssDNA-co-catalyst analyte. The expected monoisotopic mass for the conjugate, including the 26-nucleotide single-stranded DNA dna07 and a single 4,4′-dicarboxybipyridine (dcbpy) co-catalyst bound at the 5′-terminus, is shown. The observed monoisotopic mass, calculated by deconvolution of the observed $z = -14$ precursor (m/z = 597.2424), is also shown. Moderately abundant adducted species, including the expected conjugate with sodium and ammonium adducts, as well as a minor double addition impurity, are additionally labeled.

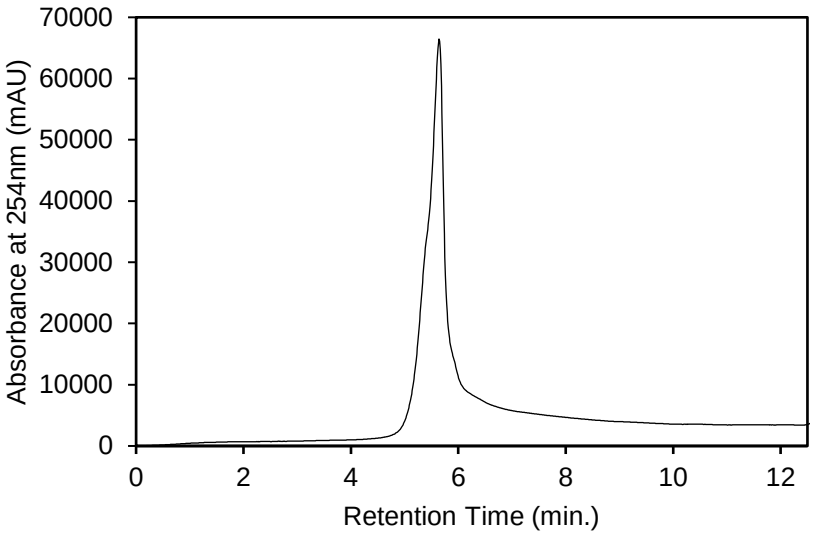

Figure S8. HPLC chromatogram of HPLC-purified dna15+dcbpy using absorbance at 254 nm. 10 μL of 0.2x DNA-conjugate stock were injected for analysis.

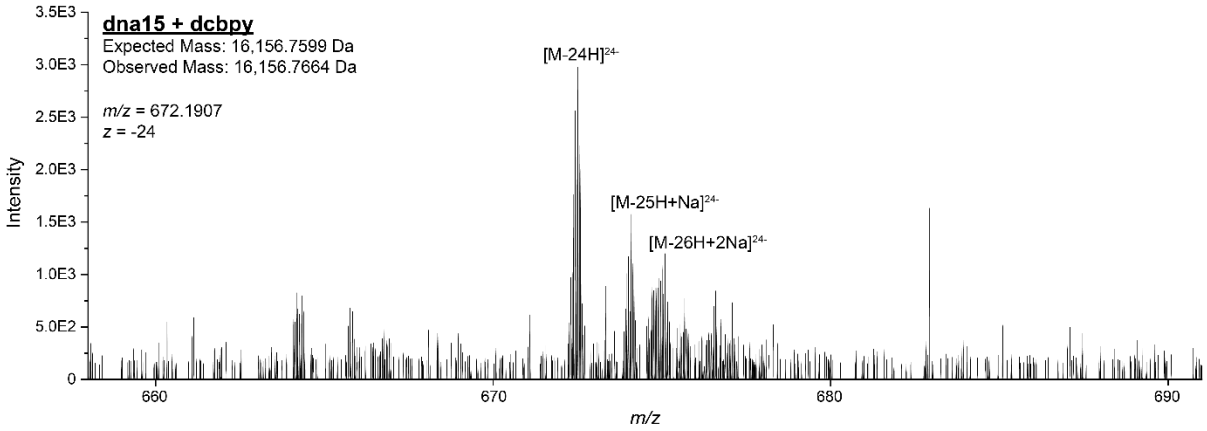

Figure S9. Electrospray mass spectrum for the HPLC-purified dna15+dcbpy conjugate**.** A negative-mode, high-resolution MS^1 spectrum, representing the average of 50 scans, is shown for the ssDNA-co-catalyst analyte. The expected monoisotopic mass for the conjugate, including the 51-nucleotide single-stranded DNA sequence dna15 and a single 4,4′-dicarboxybipyridine (dcbpy) co-catalyst bound at the 3′-terminus, is shown. The observed monoisotopic mass, calculated by deconvolution of the observed $z = -24$ precursor (m/z = 672.1907), is also shown. Moderately abundant adducted species, including the expected conjugate with sodium and ammonium adducts, are additionally labeled.

General Procedure for Bioconjugation of a Nitroxyl Radical to DNA

Method adapted from Li et al.[3]

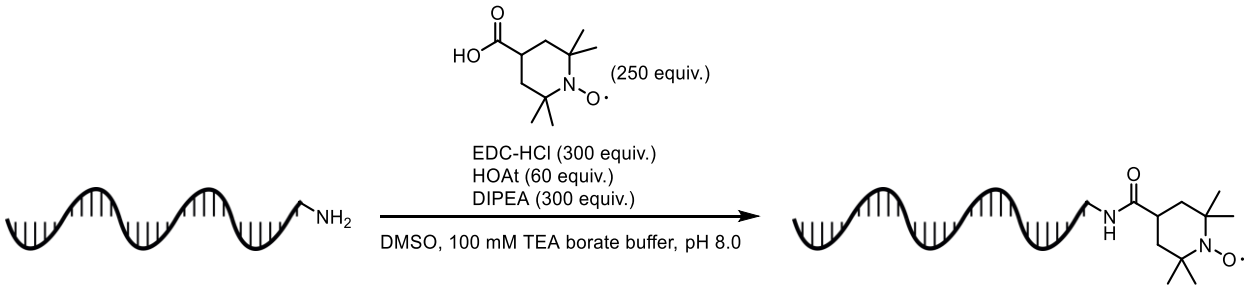

In a 1.5 mL centrifuge tube, 100 nmol of amine-modified DNA oligonucleotide (10 mM stock in nuclease-free water) was diluted with 90 μL of 100 mM triethylammonium borate buffer, pH 8.0 and 250 μL of DMSO. To this solution was added 50 μL of an 0.5 M stock of 4-carboxy-TEMPO (cTEMPO, 250 equivalents) in DMSO, 100 μL of a 0.3 M stock of EDC-HCl in DMSO (300 equivalents), 50 μL of a 0.12 M stock of HOAt in DMSO (60 equivalents) and 50 μL of a 0.6 M stock of DIPEA in DMSO (300 equivalents). The sample was then vortexed thoroughly, spun down in a benchtop microcentrifuge, and then incubated for 16 hours at room temperature without shaking. The sample was then precipitated by isopropanol precipitation (40 μL 3 M sodium acetate, 1 mL cold isopropanol, spun down at 21000 rcf at 4 °C for 30 minutes). The supernatant was decanted, and the pellet was rinsed with two 200 μL portions of cold 70% ethanol, air-dried, and resuspended to approximately 1 mM concentration with nuclease-free water. The concentration of crude DNA was then checked by UV absorption at 260 nm using a NanoDrop spectrometer. The isolated conjugate was then purified by HPLC by iterative injection of 20 nmol aliquots. The product-containing fractions were then pooled, lyophilized, and buffer-exchanged with nuclease-free water on a second Amicon Ultra filtration device to remove residual TEAA from the HPLC purification. The sample was then subjected to a final lyophilization before resuspension in nuclease free water to approximately 1 mM concentration. The final concentration of the conjugate stock was determined using a NanoDrop spectrometer. Yields ranged from 35–50 nmol of HPLC-purified DNA conjugate. To assess the integrity of oligonucleotide-co-catalyst conjugates, intact mass analysis via electrospray mass spectrometry (ESI-MS) was performed (see "Mass Spectrometry").

Characterization of TEMPO-DNA Conjugates

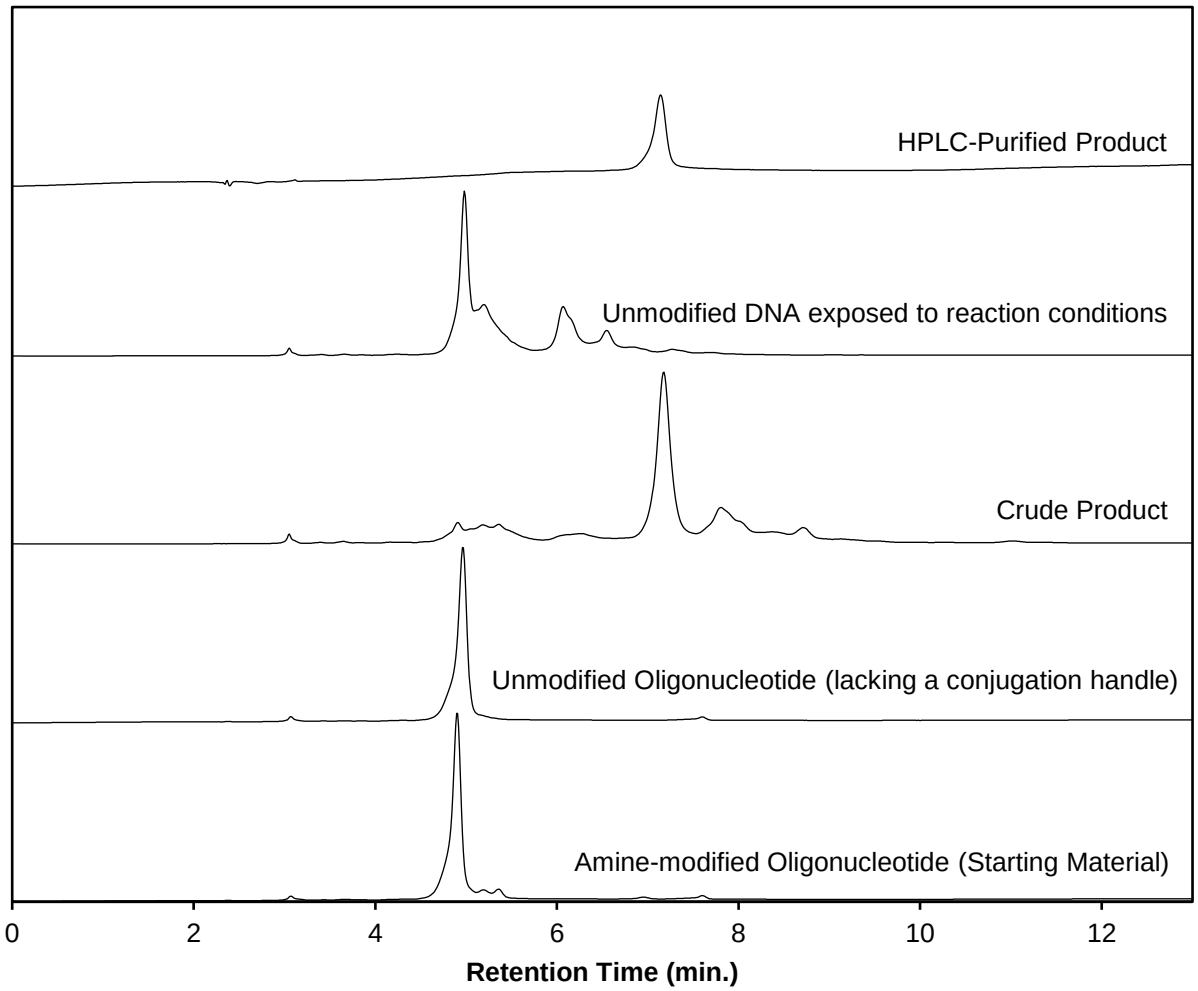

Figure S10. HPLC Analysis of the bioconjugation of 4-carboxy-TEMPO to DNA. Subjection of an amine-modified DNA oligonucleotide (dna06) to bioconjugation conditions led to near complete consumption of the starting material oligo and generation of one major product with a few minor impurities. The control reaction using DNA that lacks a conjugation handle (dna02) showed minor product peaks, suggesting that there is non-negligible modification of the native DNA strand, perhaps through covalent modification of nucleobase amine functional groups. Subsequent HPLC purification allowed for the isolation of the major product from these undesired, multiply-modified impurities.

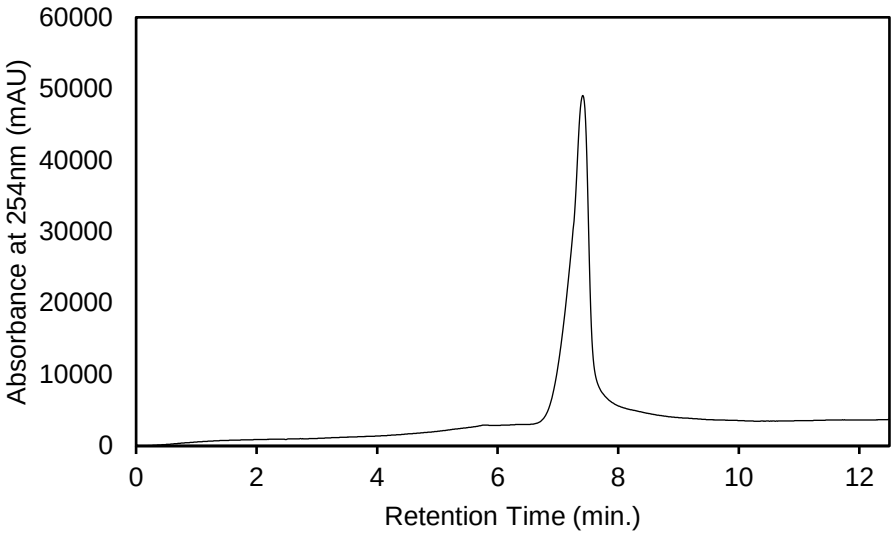

Figure S11. HPLC chromatogram of HPLC-purified dna06+cTEMPO using absorbance at 254 nm. 10 μL of 0.2x DNA-conjugate stock were injected for analysis.

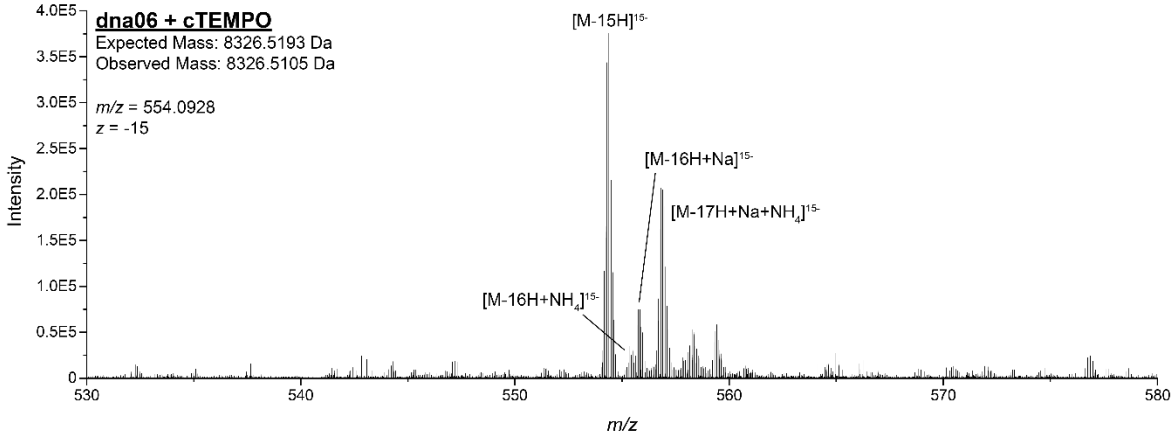

Figure S12. Electrospray mass spectrum for the HPLC-purified dna06+cTEMPO conjugate. A negative-mode, high-resolution MS^1 spectrum, representing the average of 50 scans, is shown for the ssDNA-co-catalyst analyte. The expected monoisotopic mass for the conjugate, including the 26-nucleotide single-stranded DNA sequence dna06 and a single 4-carboxy-TEMPO (cTEMPO) co-catalyst bound at the 5′-terminus, is shown. The observed monoisotopic mass, calculated by deconvolution of the observed $z = -15$ precursor (m/z = 554.0928), is also shown. Moderately abundant adducted species, including the expected conjugate with sodium and ammonium adducts, are additionally labeled.

Synthesis of 6-methoxy-2-naphthalenemethanol

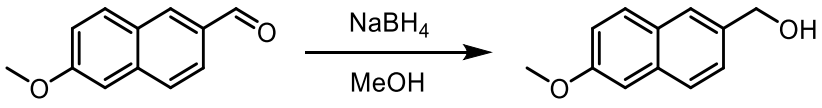

89.6% yield

6-methoxy-2-naphthaldehyde (2 g, 10.7 mmol, 1 equivalent) was dissolved in 50 mL HPLC-grade methanol (no precautions were taken to dry the solvent) in a 100 mL round-bottom flask with stirring. Sodium borohydride (0.450 g, 11.9 mmol, 1.1 equivalents) was then added in 50 mg portions (vigorous bubbling was observed after each addition, and the color of the reaction mixture changed from clear orange to a yellow-green). 2 mL of methanol were used to rinse residual sodium borohydride from the edges of the flask into the mixture, the reaction was placed under a nitrogen atmosphere and stirred at room temperature until complete consumption of the aldehyde was observed by TLC (5% ethyl acetate in hexanes, with visualization by UV and $KMnO_4$ staining). The solvent was then removed under reduced pressure and resulting off-white solid was redissolved in 50 mL of ethyl acetate. The organic layer was then partitioned with 20 mL of a saturated aqueous solution of ammonium chloride and 20 mL of distilled water. The aqueous layer was extracted with 3×20 mL ethyl acetate, and all organic layers were combined. The organic layers were then washed with 10 mL distilled water followed by 10 mL brine. The combined organic layers were dried over anhydrous magnesium sulfate, filtered and the solvent was removed under reduced pressure. This yielded 1.80 g (89.6% yield) of product as a beige powder. The structure was confirmed by ^{1}H- and ^{13}C-NMR.

^{1}H-NMR (500 MHz, $CDCl_3$) δ 7.76–7.70 (m, 3H), 7.45 (dd, *J* = 8.5, 1.7 Hz, 1H), 7.18–7.11 (m, 2H), 4.82 (s, 2H), 3.92 (s, 3H), 1.72 (s, 1H). ^{13}C NMR (126 MHz, $CDCl_3$) δ 157.76, 136.06, 134.14, 129.37, 128.82, 127.22, 125.88, 125.59, 119.02, 105.76, 77.27, 77.02, 76.77, 65.59, 55.31.

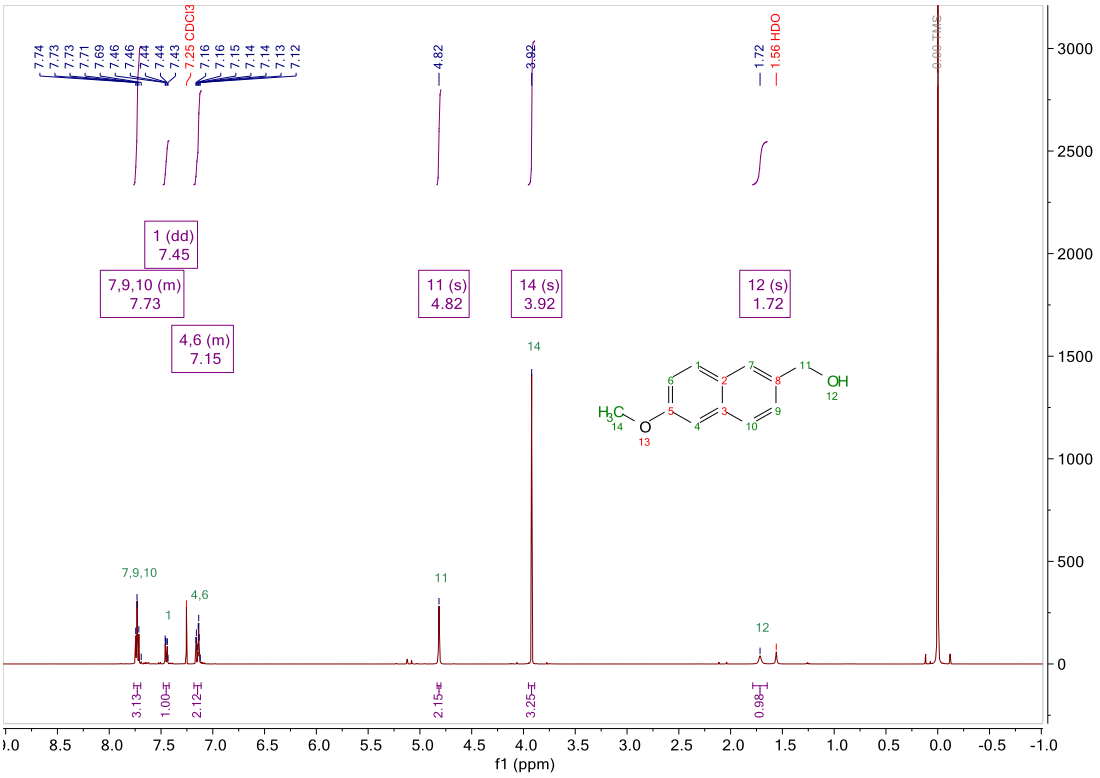

Figure S13. ^{1}H-NMR Spectrum of 6-methoxy-2-naphthalenemethanol in $CDCl_3$ (500 MHz).

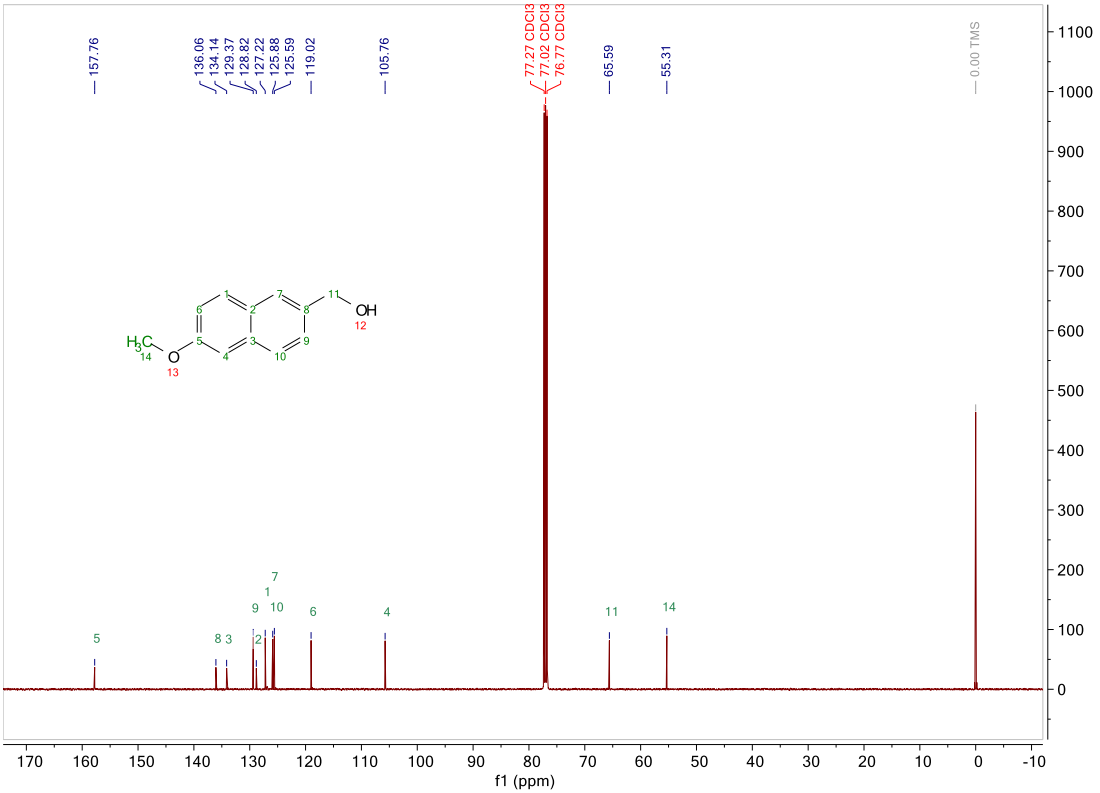

Figure S14. ^{13}C-NMR Spectrum of 6-methoxy-2-naphthalenemethanol in $CDCl_3$ (126 MHz).

Supplemental Experiments

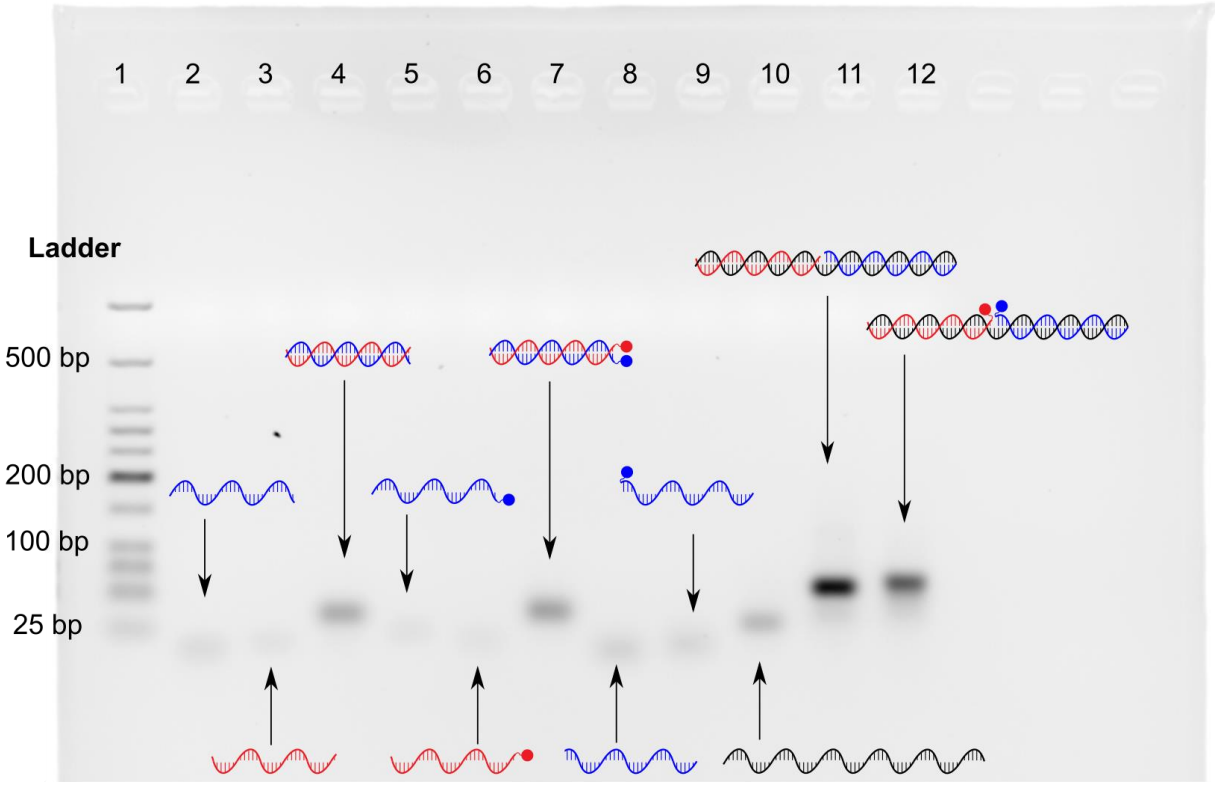

dna01:	+	-	+	-	-	-	-	-	-	-	-
dna02:	-	+	+	-	-	-	-	-	-	+	-
dna05+dcbpy:	-	-	-	+	-	+	-	-	-	-	-
dna06+cTEMPO:	-	-	-	-	+	+	-	-	-	-	+
dna03:	-	-	-	-	-	-	+	-	-	+	-
dna08+dcbpy:	-	-	-	-	-	-	-	+	-	-	+
dna09:	-	-	-	-	-	-	-	-	+	+	+

Figure S15. Agarose gel electrophoresis of DNA-scaffolded catalyst structures after annealing. The gel shows high yield of annealed product for each architecture investigated. Multi-strand structures (lanes 4, 7, 11–12) were annealed in 100 mM NaCl, 100 mM borate buffer, pH 9.5. After annealing, the samples were diluted to 1 μM concentration with nuclease-free water. Single-stranded controls (lanes 2-3, 5-6, 8-10) were not subjected to the annealing process and were loaded at 1 μM concentration.

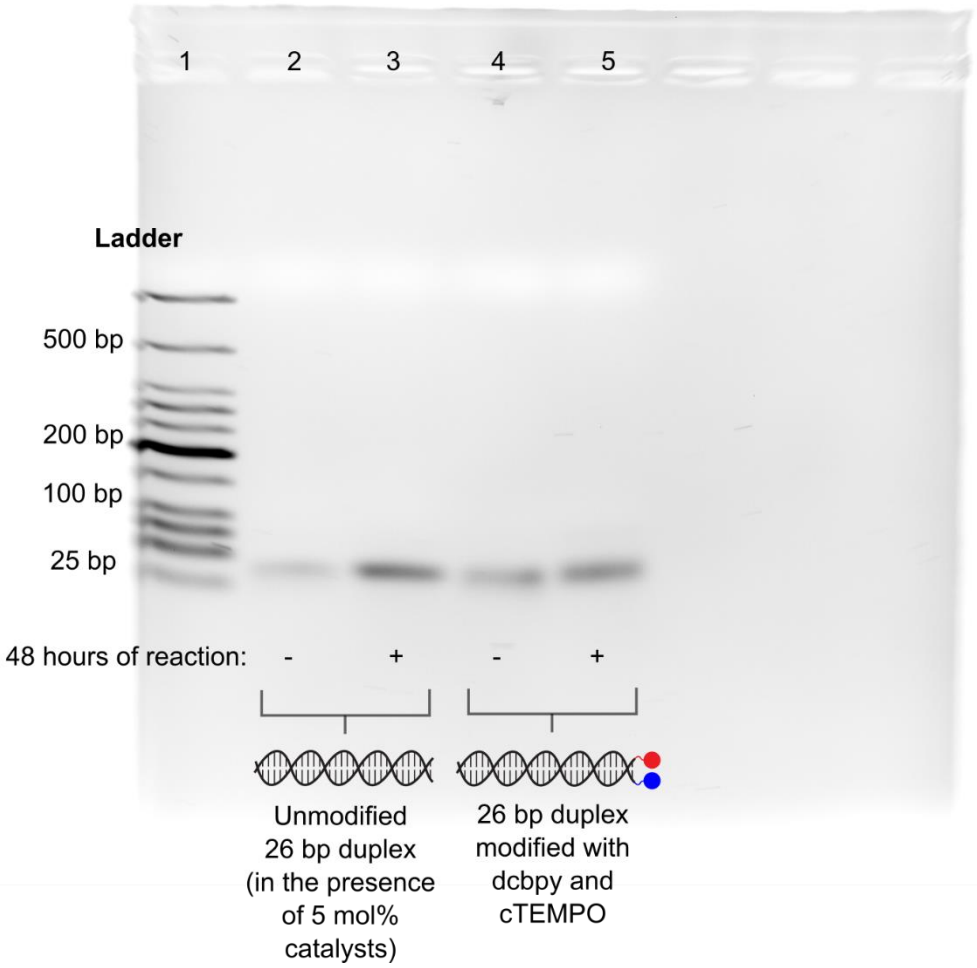

Figure S16. Agarose gel electrophoresis analysis of the DNA compatibility of the Cu/TEMPO reaction. No fragments or changes in mobility were observed for either unmodified DNA (incubated in the presence of 5 mol % CuBr, dcbpy, and carboxy-TEMPO) or 0.5 mol % scaffolded DNA-co-catalyst conjugates after 48 hours of reaction. All samples were thermally annealed (2 minutes at 92 °C, followed by cooling to room temperature) in the presence of 100 mM NaCl. DNA was recovered from the reaction by isopropanol precipitation, followed by resuspension of the pellet to 1 μM concentration (to match the concentration of the control samples). The DNA used in lanes 2 and 3 are dna01 and dna02, while the conjugates used in lanes 4 and 5 are dna05+dcbpy and dna06+cTEMPO. This observation agrees with the DNA-compatibility observed by Matsushita et al.[4]

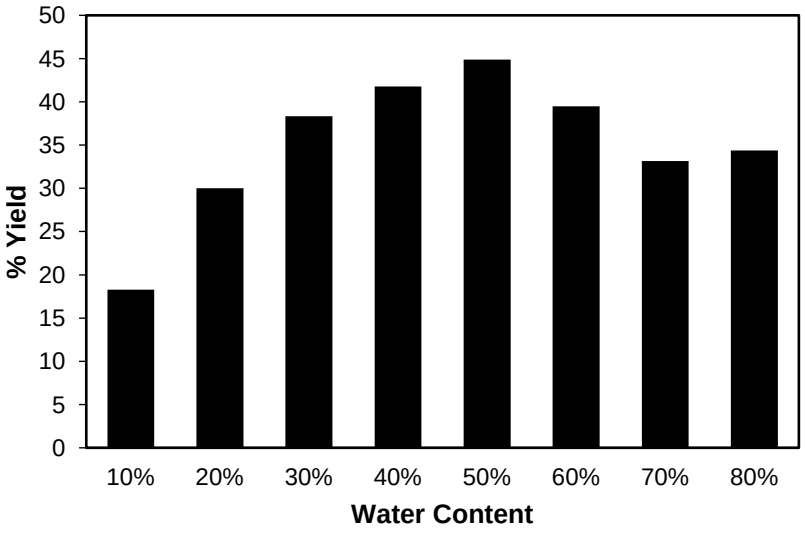

Figure S17. Optimization of semi-aqueous solvent system for the Cu/TEMPO catalyzed oxidation of benzyl alcohol. The highest yield was obtained with a 1:1 mixture of aqueous buffer and acetonitrile. Reaction conditions were 100 mM benzyl alcohol, 5 mol % TEMPO, 5 mol % 2,2′-bipyridine, 5 mol % CuBr in a mixture of 100 mM triethylammonium borate buffer pH 9.5 and acetonitrile. 1 μL aliquots were diluted to 100 μL with MeOH after 24 minutes and analyzed by HPLC to determine yield. Semi-aqueous acetonitrile solvent systems have been previously reported for Cu/TEMPO oxidations.[5]

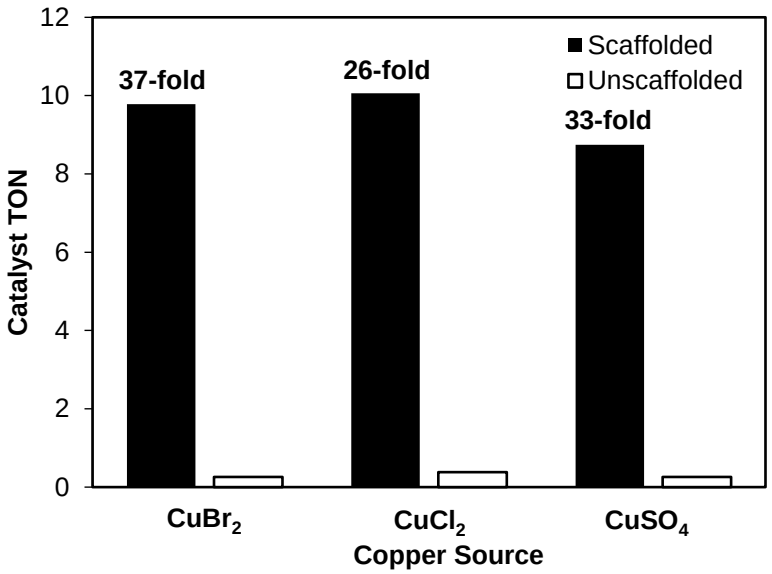

Figure S18. Comparing the catalyst turnover number of the scaffolded and unscaffolded co-catalysts (at 0.5 mol % loading) for benzyl alcohol oxidation in a purely aqueous solvent after 33.5 hours of reaction. The fold increase afforded by the scaffold relative to the unscaffolded reaction is shown for each copper source. The scaffolding enhancement remains high (ca. 30-fold) even though the absolute reactivity of the system is dramatically reduced. TON was calculated from the HPLC yield after dilution of the reaction mixture with methanol to solubilize the benzaldehyde product. Reaction conditions were 10 mM benzyl alcohol, 0.5 mol % TEMPO and 0.5 mol % 4,4′-dicarboxy-2,2′-bipyridine or 0.5 mol % scaffolded catalyst duplex, 0.5 mol % Cu(II) source, in 50 mM sodium borate buffer pH 9.5 with 50 mM NaCl.

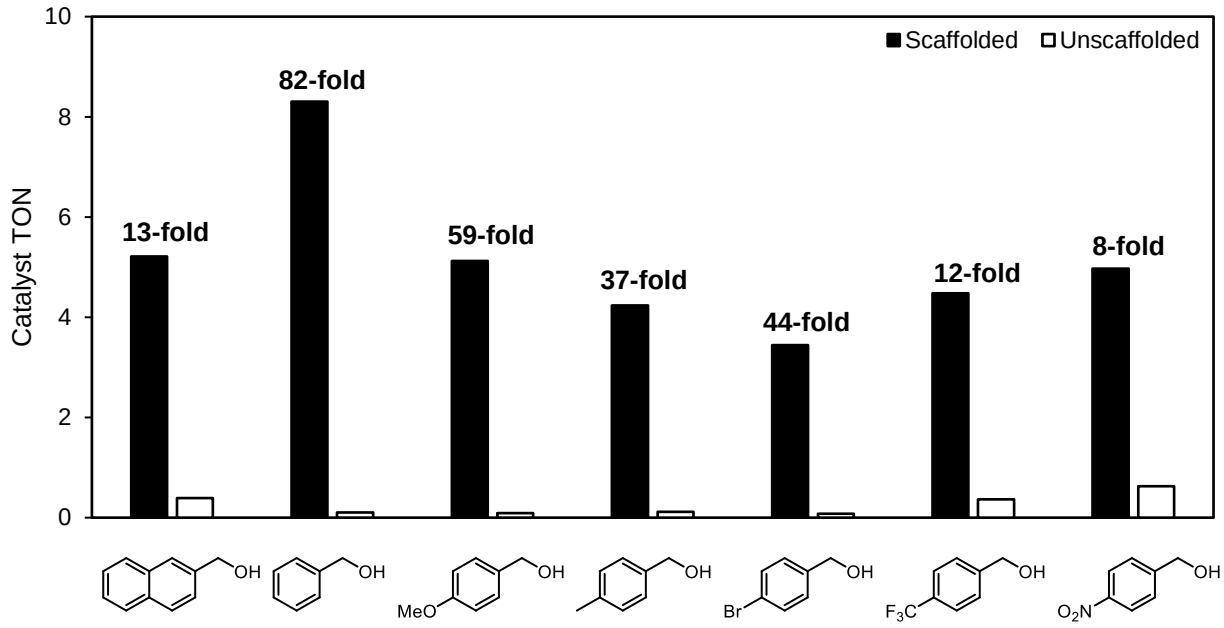

Figure S19. Comparison of scaffolded and unscaffolded oxidation of various benzylic alcohols after 4.75 hours of reaction. The fold increase afforded by the scaffold relative to the unscaffolded reaction is shown for each substrate. The scaffolding effect is observed with each substrate, suggesting that the enhancement is not due to substrate-specific interactions with the DNA scaffold. Reaction conditions were 10 mM substrate, 0.5 mol % DNA-scaffolded co-catalysts (scaffolded) or 0.5 mol % dcbpy and 0.5 mol % cTEMPO (unscaffolded), 0.5 mol % CuBr, in 1:1 MeCN/100 mM sodium borate buffer pH 9.5 with 100 mM NaCl.

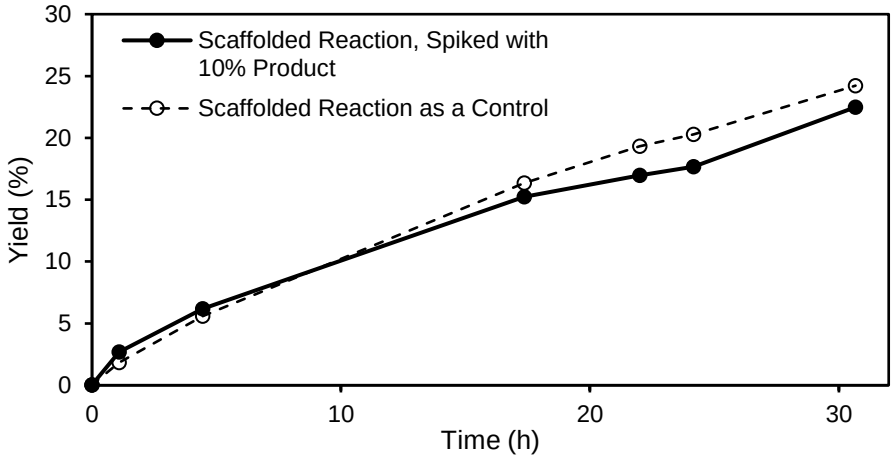

Figure S20. The effect of 10 % oxidation product on the rate of alcohol oxidation by scaffolded co-catalysts. The similarity of the product-spiked reaction profile with that of the control reaction suggests that product inhibition is not responsible for gradually decreasing reaction rate. Reaction conditions were 10 mM substrate, 0.5 mol % DNA-scaffolded co-catalysts, 0.5 mol % CuBr, in 1:1 MeCN/100 mM sodium borate buffer pH 9.5 with 100 mM NaCl.

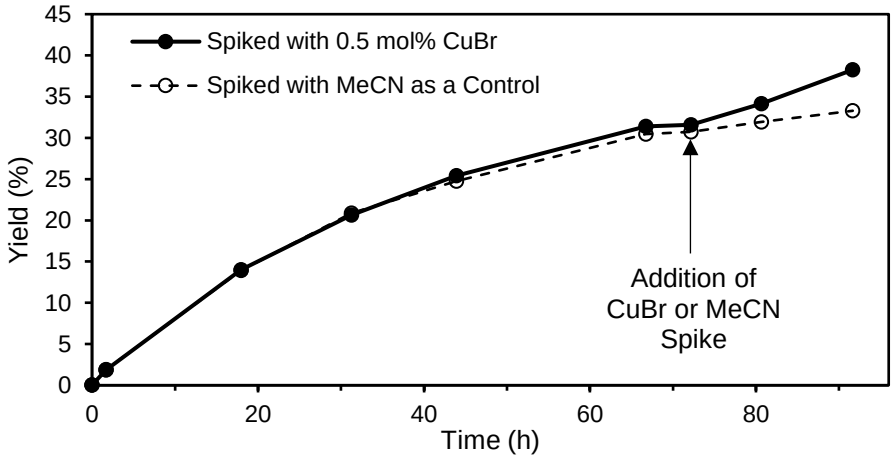

Figure S21. The effect of spiking in another aliquot of 0.5 mol % CuBr after the scaffolded reaction yield has begun to plateau. A control was run in which an equivalent volume of MeCN was spiked into the reaction. The observed partial restoration of activity after the CuBr spike suggests that the decrease in rate over time may be due to a copper-related co-catalyst deactivation pathway such as copper (II) hydroxide precipitation.[6] Reaction conditions were 10 mM substrate, 0.5 mol % DNA-scaffolded co-catalysts, 0.5 mol % CuBr, in 1:1 MeCN/100 mM sodium borate buffer pH 9.5 with 100 mM NaCl.

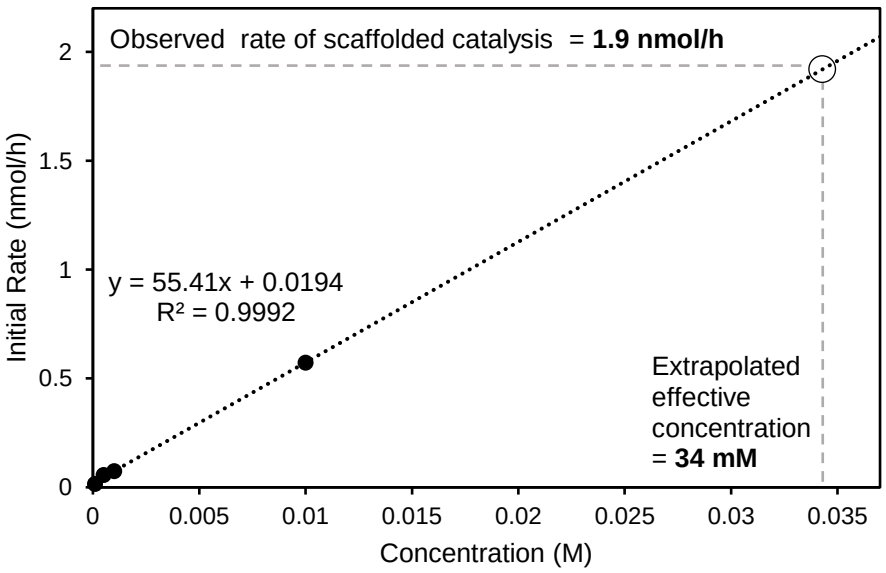

Figure S22. Calibration curve to determine the effective concentration of the nitroxyl radical co-catalyst when scaffolded on DNA. 2 nmol of DNA-linked dcbpy were incubated with 2 nmol of CuBr and varying concentrations of TEMPO as a co-catalyst. The resulting linear regression, shown above, was used to extrapolate the effective concentration of the nitroxyl radical on DNA from the observed rate of catalysis using scaffolded co-catalysts. Reaction conditions were 10 mM 2-naphthalenemethanol, 0.5 mol % DNA-dcbpy (with complementary unmodified strand), 0.5 mol % CuBr, and varied loadings of TEMPO in 1:1 MeCN/100 mM sodium borate buffer pH 9.5 with 100 mM NaCl.

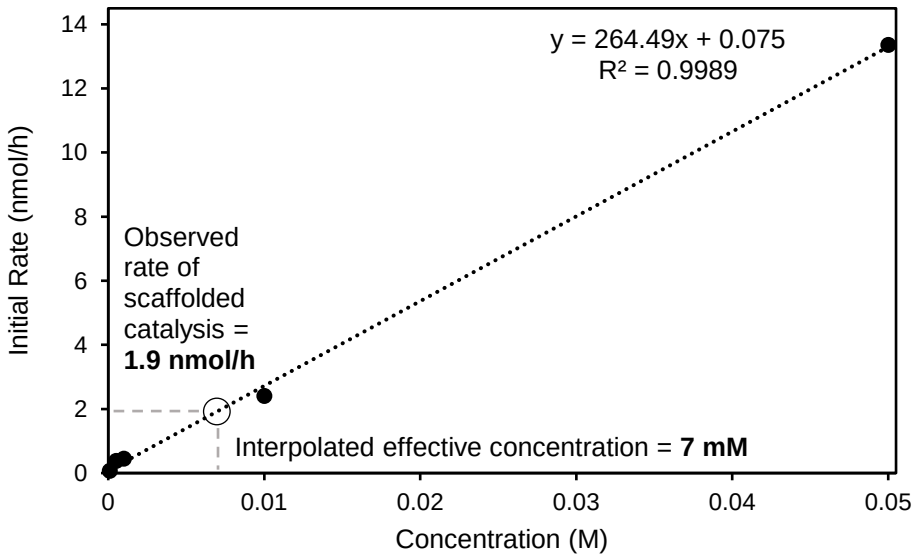

Figure S23. Calibration curve to determine the effective concentration of the 4,4′-dicarboxy-2,2′-bipyridine-Cu co-catalyst when scaffolded on DNA. 2 nmol of DNA-linked cTEMPO were incubated with varying concentrations of CuBr and dcbpy. The resulting linear regression, shown above, was used to interpolate the effective concentration of the dcbpy-Cu co-catalyst on DNA from the observed rate of catalysis using scaffolded co-catalysts. Reaction conditions were 10 mM 2-naphthalenemethanol, 0.5 mol % DNA-cTEMPO (with complementary unmodified strand), and varied, equimolar loadings of dcbpy and CuBr in 1:1 MeCN/100 mM sodium borate buffer pH 9.5 with 100 mM NaCl.

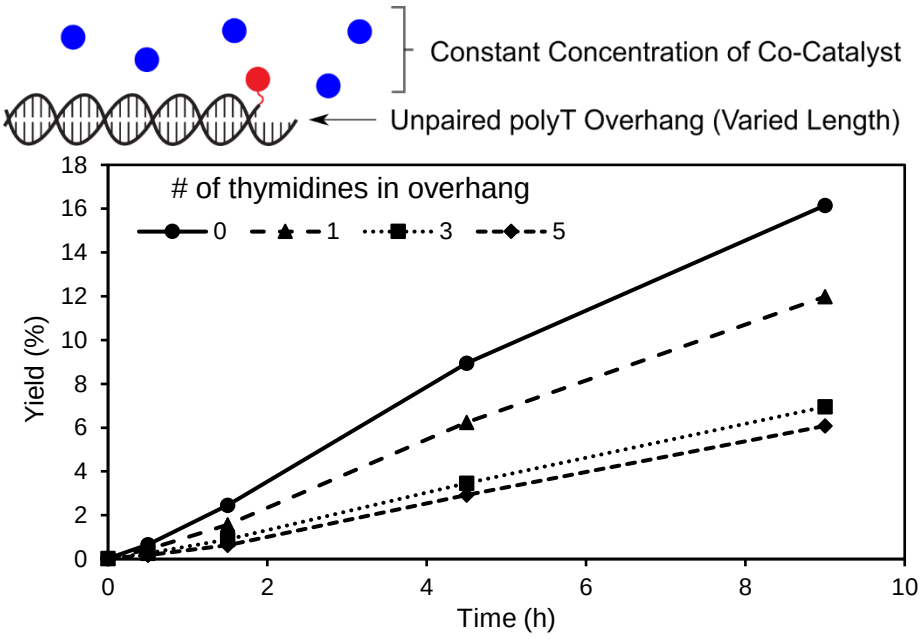

Figure S24. Unscaffolded catalysis using dcbpy-DNA conjugate annealed to an unmodified strand with varying lengths of an unpaired polythymidine overhang to determine the effect of unpaired thymidines on catalysis. The concentration of TEMPO co-catalyst was constant across each reaction. Reaction conditions were 10 mM 2-naphthalenemethanol, 0.5 mol% of DNA-dcbpy (with different overhangs on the complementary strand), 0.5 mol% CuBr, and 10 mM TEMPO in 1:1 MeCN/100 mM sodium borate buffer pH 9.5 with 100 mM NaCl.

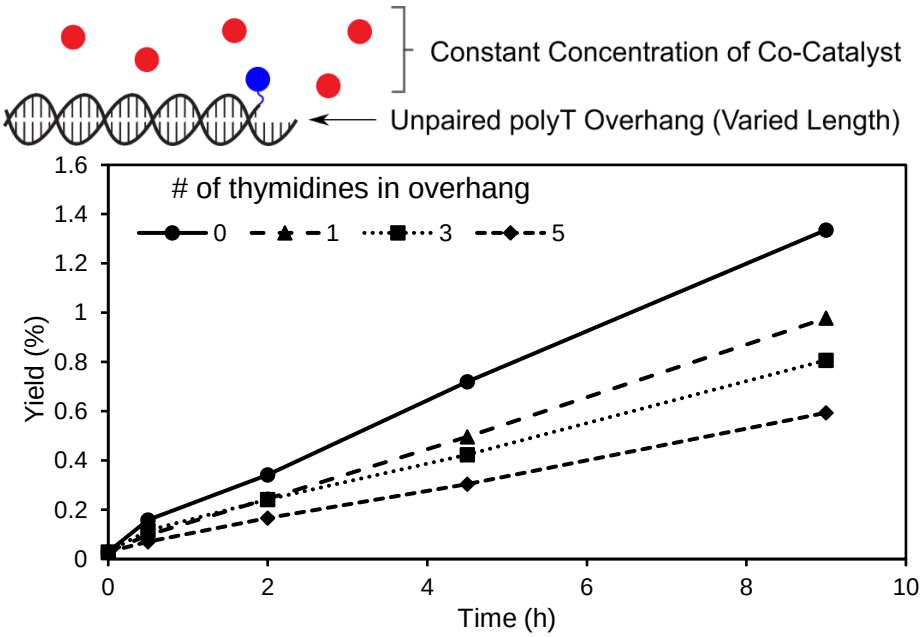

Figure S25. Unscaffolded catalysis using cTEMPO-DNA conjugate annealed to an unmodified strand with varying lengths of an unpaired polythymidine overhang to determine the effect of unpaired thymidines on catalysis. The concentrations of dcbpy and CuBr were constant across each reaction. Reaction conditions were 10 mM 2-naphthalenemethanol, 0.5 mol% of DNA-cTEMPO (with different overhangs on the complementary strand), 1mM CuBr, and 1 mM dcbpy in 1:1 MeCN/100 mM sodium borate buffer pH 9.5 with 100 mM NaCl.

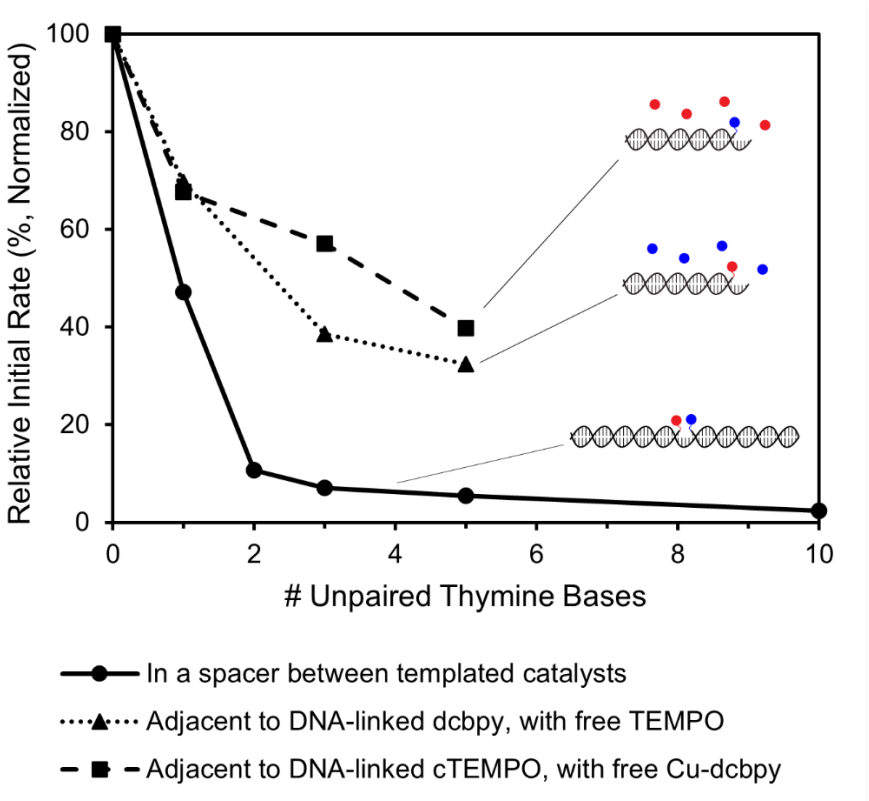

Figure S26. Comparing the effect of changing the polyT spacer length in scaffolded catalysis (data from Figure 4) with the effect of polyT overhangs on unscaffolded co-catalysts (data from Figures S24 and S25). The presence of unpaired thymidine nucleotides in proximity to the co-catalysts is detrimental to catalysis, but not enough to rationalize the decrease in rate observed in the scaffolded system with polyT spacers, suggesting that nucleobase-co-catalyst interactions and increasing inter-co-catalyst distance are both contributing factors to the observed decrease in rate of reaction in Figure 4. The initial rates are calculated from the 4.5-hour timepoint and normalized to the rate of the reaction lacking spacers/overhangs.

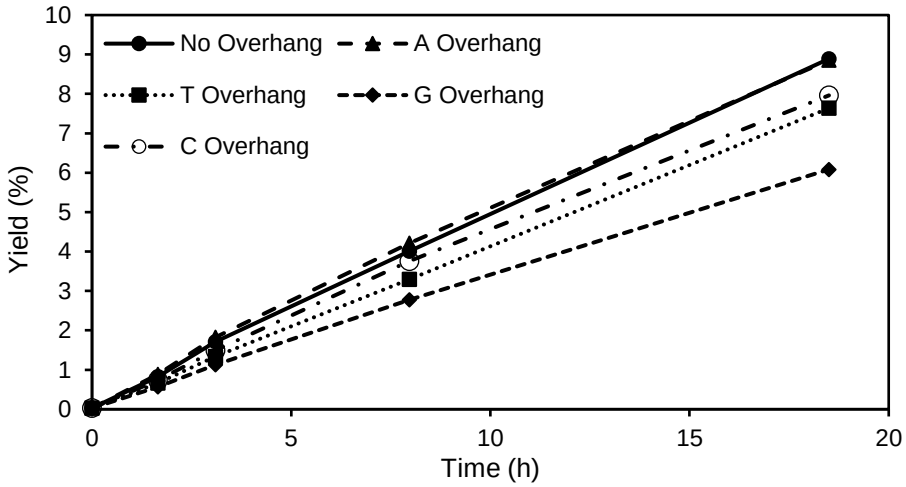

Figure S27. Comparing the effect of different unpaired nucleotides in proximity to DNA-linked dcbpy on the Cu/TEMPO catalyzed oxidation of 2-naphthalenemethanol. The presence of an unpaired T, C, or G all show moderate to minor decreases in reactivity, while the presence of an unpaired A gives little to no difference in reactivity. Reaction conditions were 10 mM 2-naphthalenemethanol, 0.5 mol% of DNA-dcbpy (with different single-nucleotide overhangs on the complementary strand), 0.5 mol% CuBr, and 10 mM TEMPO in 1:1 MeCN/100 mM sodium borate buffer pH 9.5 with 100 mM NaCl.

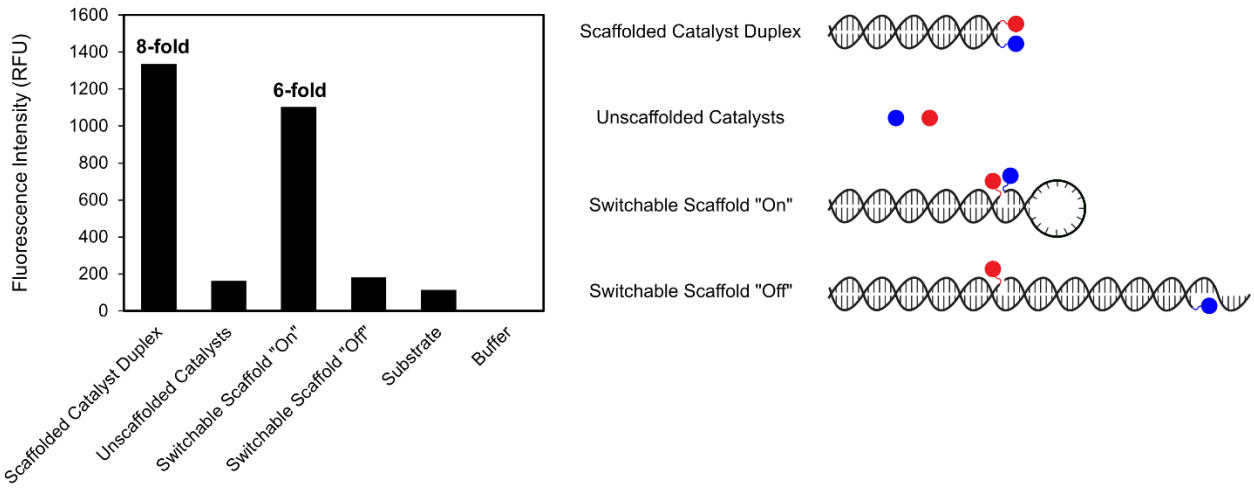

Figure S28. Fluorescence turn-on enabled by oxidation of a fluorogenic probe, 6-methoxy-2-napthalenemethanol. The fold increase in fluorescence afforded by the scaffold is indicated for the scaffolded catalyst duplex (relative to the unscaffolded reaction) and the switchable architecture in its "on" state (relative to the "off" state). Reaction conditions were 10 mM 2-naphthalenemethanol, 0.5 mol % TEMPO and 0.5 mol % 4,4′-dicarboxy-2,2′-bipyridine or 0.5 mol% scaffolded catalyst architecture (simple duplex or switchable architecture), 0.5 mol % CuBr, in 1:1 MeCN/100 mM sodium borate buffer pH 9.5 with 100 mM NaCl. The reaction was run for 45 minutes. Fluorescence was analyzed using 350 nm excitation and 450 nm emission wavelengths.

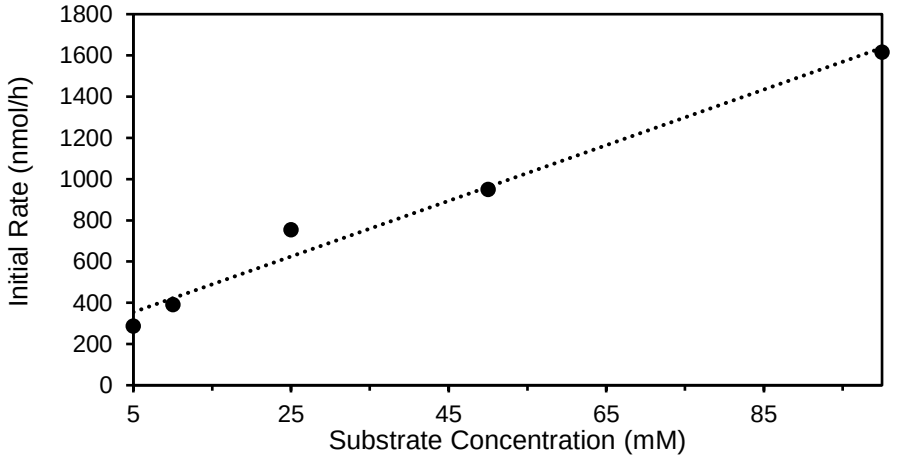

Figure S29. Initial rates experiment varying substrate loading to determine whether substrate is implicated in the rate law. Reaction conditions were 0.5 mM DNA-scaffolded co-catalysts (with an equimolar loading of CuBr) in 1:1 MeCN/100 mM sodium borate buffer pH 9.5 with 100 mM NaCl, with varied loadings of 2-naphthalenemethanol as substrate.

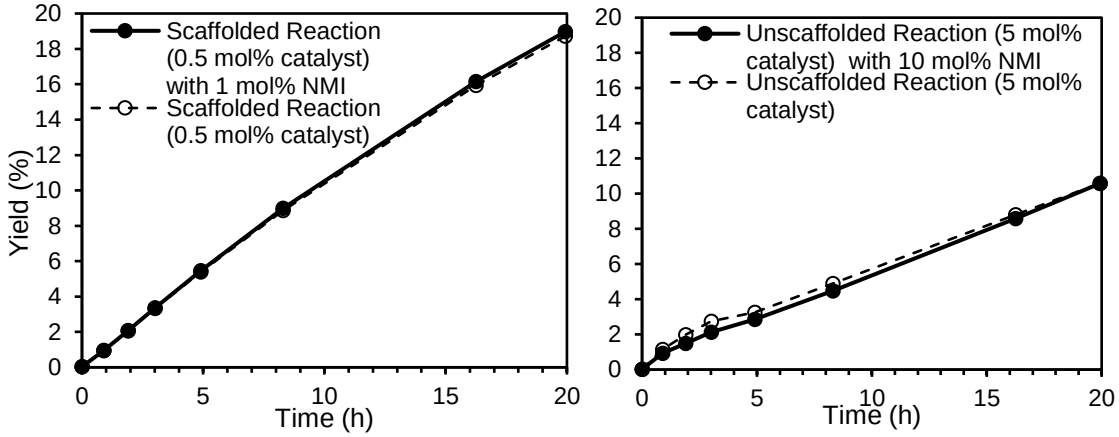

Figure S30. The effect of NMI as an additive on both the scaffolded and unscaffolded reactions (previously shown to accelerate Cu/TEMPO reactions under the conditions demonstrated by Stahl[7]). Under these dilute, semi-aqueous reaction conditions, NMI has no effect on either the scaffolded or unscaffolded reaction rate. Reaction conditions were 10 mM substrate, 0.5 mol % DNA-scaffolded co-catalysts (with an equimolar loading of CuBr) with 1 mol % NMI or 5 mol % free co-catalysts (with an equimolar loading of CuBr) with 10 mol % NMI, in 1:1 MeCN/100 mM sodium borate buffer pH 9.5 with 100 mM NaCl.

Estimating Effective Concentration

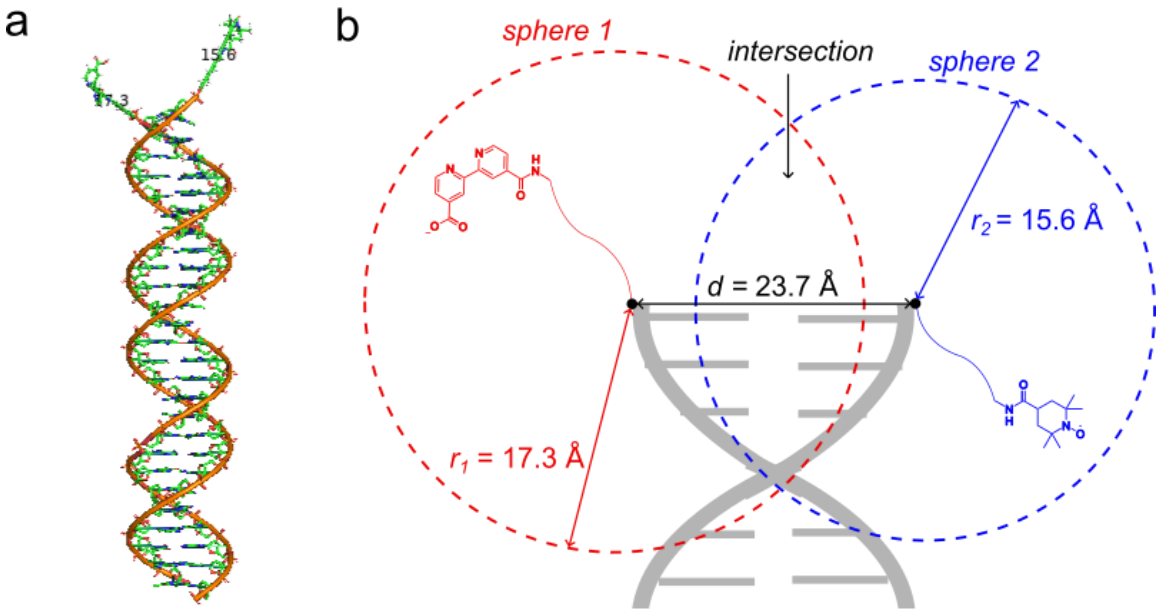

Figure S31. Estimating the effective concentration of tethered co-catalysts. (a) PyMOL model for estimating the expected effective concentration of tethered co-catalysts, no structural optimization was performed. (b) The relevant distances and spheres used to calculate the effective concentration (not to scale).

Assumptions:
To calculate the expected effective concentration using a basic theoretical model, we made the following assumptions:

1. The tethers are flexible and unrestricted (ignoring the real constraints of alkyl tethers)
2. The tether can sweep out a sphere (ignoring volume buried by DNA scaffold)
3. The distribution of co-catalyst throughout the sphere swept out by the tether is even
4. The distance between the sites of tether attachment is rigid and unmoving
5. The co-catalysts are not dynamic (ignoring Cu-ligand coordination chemistry)

These assumptions simplified the problem to the concentration of single co-catalyst molecules within two overlapping spheres (see Figure S31B).

Tethered co-catalysts were added to a DNA structure (See Figure S25A) built using PyMOL (The PyMOL Molecular Graphics System, Version 2.0 Schrödinger, LLC), and tether lengths were measured from the oxygen atom of tether attachment to the nitroxyl oxygen (for the TEMPO co-catalyst) or to the far pyridine ring of the ligand (for the dicarboxy-bipyridine ligand). The tethers were extended linearly using the "Sculpt" tool. No geometry optimization was performed on this structure.

Diameter of a B-form DNA helix (distance between attachment sites in a PyMOL-constructed DNA duplex using the "measure" tool before distortion using the "sculpt" tool) d = **23.7 Å**
Fully extended bipyridine ligand tether (from PyMOL structure) r_1 = **17.3 Å**
Fully extended nitroxyl radical tether (from PyMOL structure) r_2 = **15.6 Å**

Calculating Effective Concentration:

We defined the effective concentration in this synergistic catalytic context as the moles of co-catalyst molecule in the "intersection" volume (see Figure S31), divided by the volume (in liters) of the sphere swept out by its corresponding co-catalyst.

To calculate the effective concentration, we needed to determine the distance from the center of the spheres to the plane of intersection. We first defined the equations of the spheres, arbitrarily centered at the origin and *d* units along the x-axis:

$$x^2 + y^2 + z^2 = {r_1}^2$$

$$(x - d)^2 + y^2 + z^2 = {r_2}^2$$

We combined the two equations and solved for the *x*-coordinate of the plane of intersection:

$$(x^2 + y^2 + z^2) - ((x - d)^2 + y^2 + z^2) = {r_1}^2 - {r_2}^2$$

$$x = \frac{({r_1}^2 - {r_2}^2) + d^2}{2d}$$

$$x = 13.03 \text{ Å}$$

Next, we determined the volume of the intersection, $V_{intersection}$, by treating the intersection as two separate spherical caps. We integrated each spherical cap by disks (using *d*, r_1, r_2, and the *x*-coordinate of the plane of intersection to determine the bounds of the definite integrals) and added the two volumes:

$$V_{intersection} = V_{spherical\ cap\ 1} + V_{spherical\ cap\ 2}$$

$$V_{intersection} = \int_{8.1\text{Å}}^{13.0\text{Å}} \pi(\sqrt{{r_2}^2 - (x - d)^2})^2\, dx + \int_{13.0\text{Å}}^{17.3\text{Å}} \pi(\sqrt{{r_2}^2 - x^2})^2\, dx$$

$$V_{intersection} = 1975 \text{ Å}^3 = 1.975 \times 10^{-24}\ L$$

Next, we determined the moles of one co-catalyst within the overlapping volume, $n_{effective,\ co\text{-}catalyst\ 1}$. Assuming an even distribution of co-catalyst throughout the sphere, this is calculated by setting up a ratio of the volume of intersection and the volume of the sphere swept out by the co-catalyst's tether:

$$n_{effective,\ \ co-catalyst\ 1} = \left(\frac{1\ molecule}{N_{Avogadro}}\right) \times \left(\frac{V_{intersection}}{V_{sphere\ 1}}\right)$$

Finally, to calculate the effective concentration of one co-catalyst as seen by its co-catalyst, $C_{effective}$, we divided $n_{effective,co\text{-}catalyst\ 1}$ by the volume of the sphere swept out by the co-catalyst on its tether (ensuring that all volumes have been converted to liters). This gave a general expression for the effective concentration of scaffolded co-catalysts:

$$C_{effective} = \frac{n_{effective,\ co-catalyst\ 1}}{V_{sphere\ 2}} = \frac{1\ molecule\ \times V_{intersection}}{N_{Avogadro} \times V_{sphere\ 1} \times V_{sphere\ 2}}$$

$$C_{effective} = 0.0130\ M = \mathbf{13.0\ mM}$$

Supplemental Note: Mechanism of Cu/TEMPO Oxidation

Significant work has been done to elucidate the mechanism of the Cu/TEMPO oxidation of both activated and aliphatic alcohols. Elaboration of the mechanism of the Cu/TEMPO-catalyzed oxidation of benzylic alcohols is beyond the scope of this work. For further reading, we direct the reader to the work of Sheldon, Koskinen, Stahl, and Brückner.[6,8–11]

Differences in co-catalyst rate dependence imply a different rate-limiting step:
The mechanistic work by Stahl identifies Cu(I) reoxidation by molecular oxygen as the rate-limiting step in the oxidation of benzyl alcohol under their conditions, and demonstrates that the rate of reaction is independent of the TEMPO co-catalyst concentration and substrate concentration.[10] If this were the case for our system, increasing the effective concentration of TEMPO through scaffolding would not be expected to affect rate. In contrast to the results of Stahl and coworkers, our data show a clear rate dependence on the concentrations of copper complex, TEMPO, and substrate under our conditions for the oxidation of benzylic alcohols (Figures S22-S23, S29). Based on these data we hypothesize that the substrate oxidation step is rate-limiting under our conditions, and that the scaffolding effect increases rate through increased effective co-catalyst concentration.

Intermediacy of dimeric Cu(I) species:
Previous mechanistic work posits the role of dimeric Cu intermediates in co-catalyst reoxidation under certain conditions,[9,10] although there is disagreement in the literature on this point.[11] In contrast to the initial rates experiment reported by Stahl,[10] our data (Figure S23) suggest a first-order dependence on the (dcbpy)CuBr complex.

Role of NMI as an additive:
The use of NMI as an additive has been shown to enhance reactivity under Stahl conditions for benzyl alcohol oxidation,[7] likely by accelerating the slow Cu(I)-reoxidation step through coordination to the catalytic Cu center.[10,11] Under our conditions, addition of NMI does not affect the rate of reaction regardless of the presence of DNA (Figure S30). A possible mechanistic explanation for this distinction between the Stahl conditions and our conditions is that NMI may only serve to accelerate reactions in which Cu(I) reoxidation is rate-limiting.

References

(1) Peters-Clarke, T. M.; Quan, Q.; Brademan, D. R.; Hebert, A. S.; Westphall, M. S.; Coon, J. J. Ribonucleic Acid Sequence Characterization by Negative Electron Transfer Dissociation Mass Spectrometry. *Anal. Chem.* **2020**, *92* (6), 4436–4444. https://doi.org/10.1021/acs.analchem.9b05388.

(2) Peters-Clarke, T. M.; Schauer, K. L.; Riley, N. M.; Lodge, J. M.; Westphall, M. S.; Coon, J. J. Optical Fiber-Enabled Photoactivation of Peptides and Proteins. *Anal. Chem.* **2020**, *92* (18), 12363–12370. https://doi.org/10.1021/acs.analchem.0c02087.

(3) Li, Y.; Gabriele, E.; Samain, F.; Favalli, N.; Sladojevich, F.; Scheuermann, J.; Neri, D. Optimized Reaction Conditions for Amide Bond Formation in DNA-Encoded Combinatorial Libraries. *ACS Comb Sci* **2016**, *18* (8), 438–443. https://doi.org/10.1021/acscombsci.6b00058.

(4) Matsushita, T.; Moriyama, Y.; Nagae, G.; Aburatani, H.; Okamoto, A. DNA-Friendly Cu(II)/TEMPO-Catalyzed 5-Hydroxymethylcytosine-Specific Oxidation. *Chem. Commun.* **2017**, *53* (42), 5756–5759. https://doi.org/10.1039/C7CC02814H.

(5) Gamez, P.; Arends, I. W. C. E.; Reedijk, J.; Sheldon, R. A. Copper(II)-Catalysed Aerobic Oxidation of Primary Alcohols to Aldehydes. *Chem. Commun.* **2003**, No. 19, 2414–2415. https://doi.org/10.1039/B308668B.

(6) Hoover, J. M.; Ryland, B. L.; Stahl, S. S. Copper/TEMPO-Catalyzed Aerobic Alcohol Oxidation: Mechanistic Assessment of Different Catalyst Systems. *ACS Catal.* **2013**, *3* (11), 2599–2605. https://doi.org/10.1021/cs400689a.

(7) Hoover, J. M.; Stahl, S. S. Highly Practical Copper(I)/TEMPO Catalyst System for Chemoselective Aerobic Oxidation of Primary Alcohols. *J. Am. Chem. Soc.* **2011**, *133* (42), 16901–16910. https://doi.org/10.1021/ja206230h.

(8) Gamez, P.; Arends, I. W. C. E.; Sheldon, R. A.; Reedijk, J. Room Temperature Aerobic Copper–Catalysed Selective Oxidation of Primary Alcohols to Aldehydes. *Advanced Synthesis & Catalysis* **2004**, *346* (7), 805–811. https://doi.org/10.1002/adsc.200404063.

(9) Kumpulainen, E. T. T.; Koskinen, A. M. P. Catalytic Activity Dependency on Catalyst Components in Aerobic Copper–TEMPO Oxidation. *Chemistry – A European Journal* **2009**, *15* (41), 10901–10911. https://doi.org/10.1002/chem.200901245.

(10) Hoover, J. M.; Ryland, B. L.; Stahl, S. S. Mechanism of Copper(I)/TEMPO-Catalyzed Aerobic Alcohol Oxidation. *J. Am. Chem. Soc.* **2013**, *135* (6), 2357–2367. https://doi.org/10.1021/ja3117203.

(11) Rabeah, J.; Bentrup, U.; Stößer, R.; Brückner, A. Selective Alcohol Oxidation by a Copper TEMPO Catalyst: Mechanistic Insights by Simultaneously Coupled Operando EPR/UV-Vis/ATR-IR Spectroscopy. *Angewandte Chemie International Edition* **2015**, *54* (40), 11791–11794. https://doi.org/10.1002/anie.201504813.